~~Vegetation health monitoring based on~~ Detection of tree stress from sub-daily sap flow variability

Anna T. Schackow[1,2], Susan C. Steele-Dunne[3], David T. Milodowski[4], Jean-Marc Limousin[5], and Ana Bastos[1,2]

[1]Institute for Earth System Science and Remote Sensing, Leipzig University, Germany
[2]Max Planck Institute for Biogeochemistry, Dept. of Biogeochemical Integration, Jena, Germany.
[3]Department of Geoscience and Remote Sensing, Delft University of Technology, the Netherlands
[4]School of GeoSciences, University of Edinburgh, Edinburgh UK
[5]4 CEFE, Univ Montpellier, CNRS, EPHE, IRD, Montpellier, France

Correspondence: Anna Schackow (a.schackow@studserv.uni-leipzig.de), Ana Bastos (ana.bastos@uni-leipzig.de)

Abstract. The terrestrial biosphere plays a critical role in regulating carbon and water fluxes. Rising global temperatures increase atmospheric dryness, which in turn raises atmospheric water demand on vegetation and places. Some plants regulate transpiration losses by closing stomata, at the cost of reduced carbon uptake. Quantifying stomatal regulation and detecting early onset of vegetation stress at large scales remains a challenge.

Sap flow in stems responds to water potential gradients between the roots and the atmosphere, and therefore provides a window into transpiration and stomatal regulation. ~~Here,~~ Based on SAPFLUXNET measurements of sap flow across tropical, temperate and boreal biomes, we demonstrate how variations in the diurnal cycle of ~~sub-daily~~ sap flow as a function of vapor pressure deficit (VPD) measurements can elucidate the different levels of plant hydraulic stress. We derive two metrics based on sub-daily responses of sap flow to VPD: the morning sensitivity, given by the slope of the bi-variate relationship, and the area of the diurnal sap flow – VPD curve. We find that seasonal variations in the morning slope ~~, is~~ are positively associated with top soil moisture (0-30cm)~~soil moisture, i.e., soil water availability~~. The area of the diurnal cycle, characterizing the degree of daily hysteresis between sap flow and VPD, ~~is sensitive to temperature and soil moisture, increasing~~ increases with sap flow downregulation before peak VPD and is sensitive to temperature and soil moisture variability at seasonal time scales.

While in situ sensors can provide continuous sap flow data, we ~~consider~~ aim to evaluate the potential to estimate ~~these~~ descriptors of the diurnal cycle using temporally sparse data. In particular, as sap flow is connected to changes in water storage, which can be estimated using microwave remote sensing, we examine the degree to which the slope and area can be estimated for several acquisition strategies that vary in terms of the numbers of observations and acquisition times. We ~~argue~~ propose that sub-daily microwave observations, with at least three sub-daily overpasses could be used to characterize the sub-daily hysteresis and enable improved monitoring of ~~biosphere dynamics and vegetation health~~tree hydraulic stress and, consequently, biosphere dynamics.

1 Introduction

~~Conceptual representation of the diurnal variation in sap flow (SF, blue) and vegetation water content (VWC, orange). Hysteresis in the relationship between both quantities and vapor pressure deficit depends on environmental conditions and stress. It is hypothesized that characterizing this hysteresis with sub-daily observations at key times could provide insight into vegetation health, stress state and stress response.~~

~~Rising CO_2 levels drive rising temperatures , which in turn~~ Rising temperatures under global warming intensify the atmospheric demand for water (Vicente-Serrano et al., 2022a). This leads to reduced water availability, particularly in semi-arid regions, and heightens the risk of plant hydraulic stress or even hydraulic failure (Allen et al., 2015; Vicente-Serrano et al., 2022b). Climate change thus poses a significant threat to global vegetation health (Hartmann et al., 2022), raising serious concerns about ecosystem stability and the planet's ability to regulate climate (Bustamante et al., 2023).

~~Plant-water dynamics is a fundamental indicator of~~ Water plays a fundamental role in plant functioning, ~~connecting the carbon, water and energy cycles~~acting as a reactant in photosynthesis, regulating cell turgor and nutrient transport, and supporting evaporative cooling under hot temperatures. Water loss through evaporation in the stomata (transpiration) reduces ~~the~~ leaf water potential, inducing the flow of sap from the soil through the root-stem-leaf continuum (sap flow, SF) and supporting the transport of nutrients through the xylem (Hammond et al., 2021). Regulation of stomatal aperture (stomatal conductance) allows plants to respond to changes in environmental conditions in order to preserve the continuity of the plant water column (Jarvis and McNaughton, 1986a) and avoid embolism (Hammond et al., 2021)~~,~~.

Vegetation water dynamics provides critical insights into plant functioning and connect the carbon, water and energy cycles at time-scales from ~~seconds to seasons or longer (Konings et al., 2021).~~ hours to decades. At longer time-scales (seasonal to interannual), variations in vegetation water content (VWC) typically reflect variations in vegetation biomass structure which are influenced by phenology, growth, natural disturbances and land-use (Konings et al., 2019). By contrast, vegetation water stress responses occur at time-scales from hours to months (Konings et al., 2019), with diurnal variations in vegetation water content and SF revealing signs of tree mortality several months before visual signs emerge (Hammond et al., 2021; Preisler et al., 2021).

Ecosystems have evolved varying strategies to cope with high atmospheric water demand and limited soil moisture availability. Maintaining high stomatal conductance through periods of high atmospheric water demand may increase gross carbon uptake and therefore promote faster growth, but increased rates of evapotranspiration may risk embolism and deplete water reserves if dry conditions persist (McDowell et al., 2022). Downregulation of transpiration through stomata reduces water loss, thus preserving water reserves, but also reduces the diffusion of CO_2 into the leaf, thus coming at the expense of reduced carbon uptake in the short term, and the availability of carbon for growth and plant maintenance, in the long run (Hammond et al., 2021). The outcome of these different strategies is complex and depends on multiple factors, such as drought characteristics, environmental factors, ecosystem memory and compounding effects (Cranko Page et al., 2022; Peltier and Ogle, 2023; Bastos et al., 2021) and biotic interactions (Seidl et al., 2017). Tracking the responses in vegetation water content and fluxes

to changing atmospheric conditions is crucial for understanding the vitality of global ecosystems and assessing their potential risk of mortality (Preisler et al., 2021; Hammond et al., 2021; Landsberg et al., 2017; Rowland et al., 2015) .

Vegetation undergoes daily fluctuations in water status driven by atmospheric demand, for example the high transpiration demand (VPD peak) around solar noon (Figure 1). During the growing season, plant water Diurnal fluctuations in VWC and SF reflect normal operating conditions of xylem water transport and are regulated by vegetation water storage, refilling and stomatal responses, which balance carbon uptake and transpiration-driven water loss (Jarvis and McNaughton, 1986b) . Plant water potential typically ranges from relatively high values at pre-dawn, when soil water is generally not limiting and incoming radiation is low, to lower low values during solar noon and the afternoon, particularly on clear-sky days when light and evaporative demand are high. These diel fluctuations are part of the normal operating conditions of xylem water transport and are regulated by stomatal responses, which balance carbon uptake and transpiration-driven water loss (Jarvis and McNaughton, 1986b). Healthy plants with sufficient soil water recharge their water storage available can recharge overnight, when transpiration demand is low (Forster, 2014). Increasing transpiration through the morning decreases leaf water potential, which drives a corresponding increase in SF (Tyree and Ewers, 1991). Stomatal regulation may decouple transpiration, and consequently sap flow (SF)SF, from atmospheric conditions (Franks et al., 2017)water demand (Franks et al., 2017) , giving rise to a characteristic diurnal hysteresis "loop" (Xu et al., 2022; Wan et al., 2023). In contrast, periods of prolonged drought can deplete root-zone soil moisture, reducing overnight recharge of vegetation water storage and lowering pre-dawn water content and plant water potential, leading to a certain level of stress (Davis and Mooney; Limousin et al., 2009, 2010b). We therefore hypothesise that certain characteristics of the sub-daily response of SF to VPD can help fingerprint periods and drivers of hydraulic strategies of vegetation, disentangling top-down (i.e. atmospheric demand) and bottom-up drivers (i.e. soil moisture supply) of hydraulic limitation and water use strategies.

As illustrated in Figure 1, VWC and SF usually show pronounced daily cycles, driven by atmospheric water demand (represented by vapor pressure deficit, VPD), incoming radiation, temperature, and plant hydraulic functioning. Under low-stress conditions 1(b and d), such as during spring, VWC and soil moisture are high. From pre-dawn (here represented as 6 am) to solar noon (here represented as 12 pm), VWC declines while SF increases steeply with VPD, peaking before or together with VPD. The rates of declining VWC or increasing SF indicate efficient water transport, if aligned with VPD versus active stomatal regulation, when hysteresis occurs in the diurnal cycle. SF can decrease despite rising VPD, indicating regulation in response to cumulative water loss. From mid-night to pre-dawn, SF approaches zero, and plants begin to recharge overnight, returning VWC to pre-dawn levels during the night. Under water-limited conditions, stomatal regulation reduces SF sensitivity to VPD. Morning increases in SF are muted, and VWC changes more slowly, especially in the afternoon. Pre-dawn VWC is lower due to incomplete overnight recharge. Nighttime VWC values remain low if water is not sufficiently refilled, and stress effects are more pronounced around mid-day. Under extreme stress, embolism and tissue data can result in sap flux failure, resulting in dampened sub-daily SF variability, which can be used as an early sign of tree mortality (Preisler et al., 2021; Hammond et al., 2021) . Variations in the sub-daily relationships between VWC, SF, and VPD atmospheric vapour pressure deficit (VPD) therefore provide insight into plant water regulation strategies, vegetation responses to environmental stressors and, ultimately, health.

~~Limitations in soil water supply are therefore expected to be indicated by lower sap flow rates that increase more slowly with atmospheric demand during the day as stomatal regulation restricts further transpiration losses, resulting in hysteresis loops with a lower VPD-SF gradient during the morning (Figure 1(c)). Additionally, factors like embolism, insect or fungal infestations, and disease can impair plant hydraulic conductivity (Torres-Ruiz et al.), leading to hysteresis stress signatures that may be decoupled from meteorological drivers. As sub-daily dynamics of sap flow (Figure 1 (b and c)) and vegetation water content (Figure 1 (d and e)) reflects the plant's ability to respond to abiotic stressors , both can provide an indicator of plant health andvitality. Furthermore, as water transport and stomatal regulation are near-instantaneous responses to stress conditions (Choat et al.), hydraulic hysteresis signatures potentially provide early-warning indicators that may significantly precede optically visible signs of vegetation decline (Hammond et al., 2021). We thus hypothesize that the capacity to characterize this hysteresis through sub-daily observations of SF or VWC, or proxies for them, could provide a window into vegetation healthand enable early detection of vegetation water stress before structural decline or canopy-level changes become detectable.~~

Currently, processes associated with plant ~~productivity and evapotranspiration~~ evapotranspiration and productivity are monitored at sub-daily temporal resolution in networks of sites such as FLUXNET (Pastorello et al., 2020), ICOS (RI, 2022), or SAPFLUXNET (Poyatos et al., 2021). ~~These networks cover multiple biomes and multiple years or decades for some sites, offering unique insights about carbon-water fluxes and ecosystem functioning.~~ However, these networks are relatively sparse and predominantly concentrated in North ~~American and European regions (Pastorello et al., 2020; Poyatos et al., 2021)~~ ~~.~~

~~As sap flow is driven by gradients in water potential within the vegetation, diurnal sap flow variations are closely coupled with the dynamics of vegetation water storage, considered here as vegetation water content (VWC), a quantity that can be estimated using microwave remote sensing e.g. (Konings et al., 2021; Saatchi and Moghaddam, 2000; Bernardino et al., 2024; Choudhury and Tucke . The most common~~ America and Europe (Pastorello et al., 2020; Poyatos et al., 2021). Remote-sensing plays a key role in large-scale and spatio-temporally consistent monitoring of plant water dynamics. Many studies have shown that radar observations are influenced by dynamics in VWC. A commonly used approach is to estimate VWC based on vegetation optical depth ~~, estimates of which have been obtained from many~~ from spaceborne microwave sensors (e.g. Frappart et al., 2020; Zotta et al., 2024; Konings et al., 2021). ~~Current~~ However, current and planned microwave missions provide one snapshot every few days, observing "slow" ecosystem dynamics. They are adequate to observe inter- and intra-annual variations of above ground biomass (AGB), the slow response in water status over weeks and months, and to map (a-posteriori) biomass loss due to deforestation or mortality. ~~However, this is~~This is, however, not sufficient to capture ~~the hysteresis illustrated in Figure 1 that can provide insight into~~ plant water dynamics ~~,~~ associated with health and stress as discussed above.

~~This study is motivated by the idea to use sub-daily~~ Sub-daily synthetic aperture radar (SAR) ~~to observe~~ observations have been proposed as a means for improved assessments of vegetation health and stress (e.g. Steele-Dunne et al. (2024); Matar et al. (2024)). ~~Many studies have shown that radar observations are influenced by dynamics in VWC.~~ Dawn/dusk differences have been observed in spaceborne radar backscatter from vegetated areas and attributed to variations in water status (Steele-Dunne et al., 2012; Frolking et al., 2011; Friesen, 2008; Konings et al., 2017). Daily cycles obtained by aggregating Ku-band backscat-

ter exhibit water loss/recharge patterns analogous to those illustrated in Figure 1 a) (Paget et al., 2016; Emmerik et al., 2017; Konings et al., 2017; Prigent et al., 2022). Sub-daily variations in radar observables (backscattering coefficient, coherence, phase) have been ~~observed~~ measured using tower-based radars in a range of vegetation types and conditions (Ho Tong Minh et al., 2013; Hamadi et al., 2014; Ulander et al., 2019; Ulander and Monteith, 2022; Monteith and Ulander, 2022; Ouaadi et al., 2021; Mcdonald et al., 1990; Chakir et al., 2021; Vermunt et al., 2021, 2022; Khabbazan et al., 2022), with several of the more recent studies demonstrating the link to VWC using destructive sampling, and the link to SF using co-located in-situ sensors. ~~This study will~~ Holtzman et al. (2023) have shown that increasing the number of observations from twice to four times a day could contribute to a large reduction in evapotranspiration and gross primary productivity estimated in a data-assimilation framework.

This study aims to contribute to the development of ~~such a mission~~ future sub-daily monitoring missions targeted at monitoring plant stress by providing insight into the number and timing of observations needed to ~~capture the hysteresis~~ characterize diurnal dynamics in VWC and SF as illustrated in Figure 1.

~~In this study, we investigate~~ We hypothesize that certain characteristics of the sub-daily ~~variability in sap flow and its link to diverse climate stressors, to understand whether high temporal resolution information on vegetationwater content and fluxes can be used to identify early signs of plant stress. For this, we make use of sap flow measurements from the SAPFLUXNET database (Poyatos et al., 2021) at high temporal resolution (hourly)across a wide range of biomes. We test the degree to which it is possible to capture the key characteristics of hydraulic hysteresis with targeted sub-daily measurements using experiments characterizing hysteresis in SF with plausible data acquisition strategies, which is important for understanding the minimum requirements for observation frequency if observing sub-daily hydraulic dynamics with satellites.~~

response of VWC and SF to VPD can help fingerprint periods and drivers of hydraulic strategies of vegetation, disentangle top-down (i.e. atmospheric demand) and bottom-up drivers (i.e. soil moisture supply) of hydraulic limitation and plant water use strategies (Figure 1 b–e)). Since water transport and stomatal regulation are near-instantaneous responses to stress conditions (Choat et al.), diurnal hydraulic hysteresis signatures potentially provide early-warning indicators that may significantly precede optically visible signs of vegetation decline (Preisler et al., 2021; Hammond et al., 2021). Our analysis is guided by two central research questions: (1) ~~Can plant stress be detected from the shape and dynamics of the daily sap flow cycle~~To what extent can plant responses to hydrometeorological stressors be characterized using descriptors of diurnal SF–VPD hysteresis? (2) How often, and at what times, would sparse observations be sufficient to ~~capture these stress signals?~~ estimate these descriptors?

In order to address these questions, we ~~first introduce daily metrics that describe the hysteresis in the diurnal sap flow response to atmospheric water demand. Then, we~~ investigate the sub-daily variability in the SF–VPD relationship and its link to diverse hydrometeorological stressors, based on hourly SF measurements from the SAPFLUXNET database (Poyatos et al., 2021) at high temporal resolution (hourly) across a wide range of biomes. We then propose a reduced set of descriptors that can be derived from the diurnal hysteresis cycles, and that could be estimated using comparatively sparse sub-daily observations of VWC, or some proxy for it, from satellite remote sensing. We then examine the seasonal and interannual evolution of these ~~metrics~~ descriptors at selected sites to understand how they vary in response to hydrometeorological conditions and ~~stress~~particularly extremes. Finally, we compare several observation scenarios to investigate how well these metrics could

be determined with sparser data from satellite remote sensing. We test the degree to which it is possible to capture the key characteristics of SF–VPD hysteresis with targeted sub-daily measurements using experiments characterizing hysteresis in SF with plausible data acquisition strategies, which is important for understanding the minimum requirements for observation frequency if observing sub-daily hydraulic dynamics with satellites. This would provide an opportunity for global monitoring of vegetation health and enable the early detection of vegetation stress before structural decline or canopy-level changes become detectable.

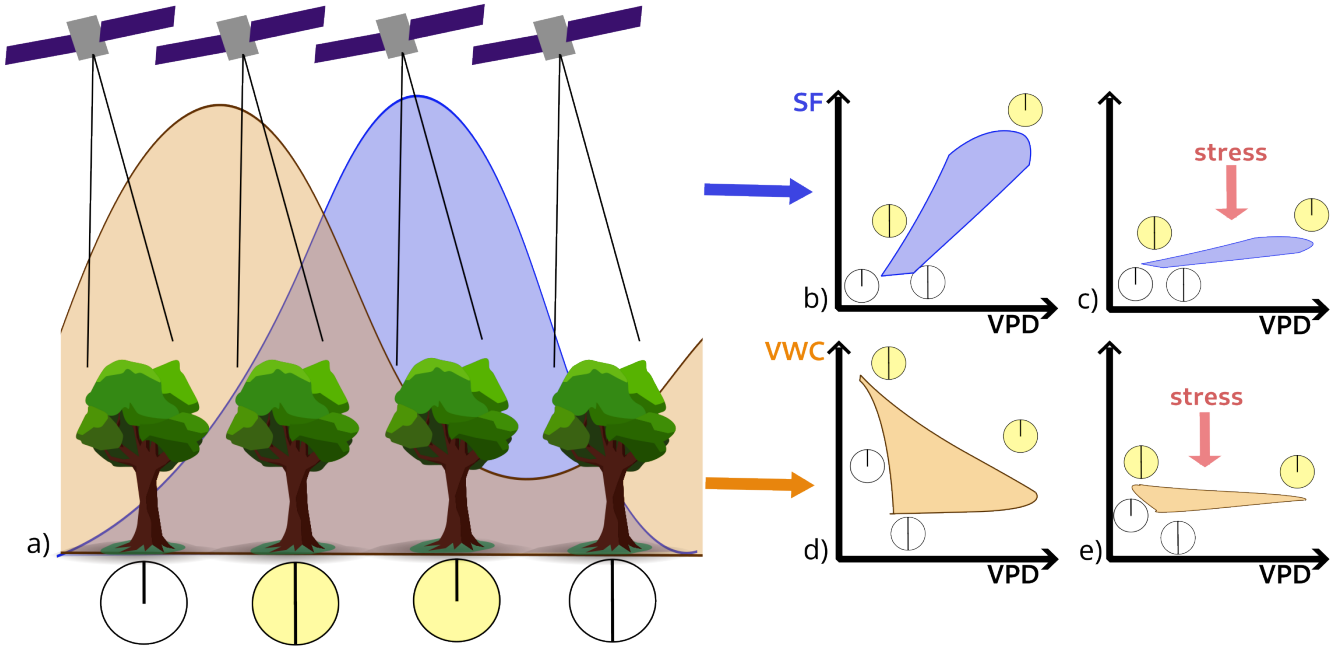

Figure 1. Conceptual representation of the diurnal variation in SF (blue) and VWC (orange). Hysteresis in the relationship between both quantities and vapor pressure deficit depends on environmental conditions and stress. It is hypothesized that characterizing this hysteresis with sub-daily observations at key times could provide insight into vegetation stress state and response. Panel a) illustrates generalized diurnal cycles of SF (blue) and VWC (orange) and the critical times of the day at which a satellite could monitor VWC (midnight, 6am, noon, 6pm, from left to right). Panels b)–e) illustrate the hypothesised diurnal relationships of SF–VPD and VWC–VPD for average conditions (b), d)) and for days marked by hydraulic stress (c), e)). The circles in panels b)–e) show the times of the day represented in panel a). The different processes driving these responses are described in Section 1.

2 Material and Methods

2.1 Data and Study Sites

The SAPFLUXNET database (Poyatos et al., 2021) provides harmonized sap flow data from forest stands across 202 sites across the globe, covering the period 1995 to 2018. The sites are primarily located in Europe and the USA, with additional sites in Australia and South Africa, and a few in the tropics and high latitude regions. Each site offers half hourly or hourly time series, with an average duration of three years (Figure 2).

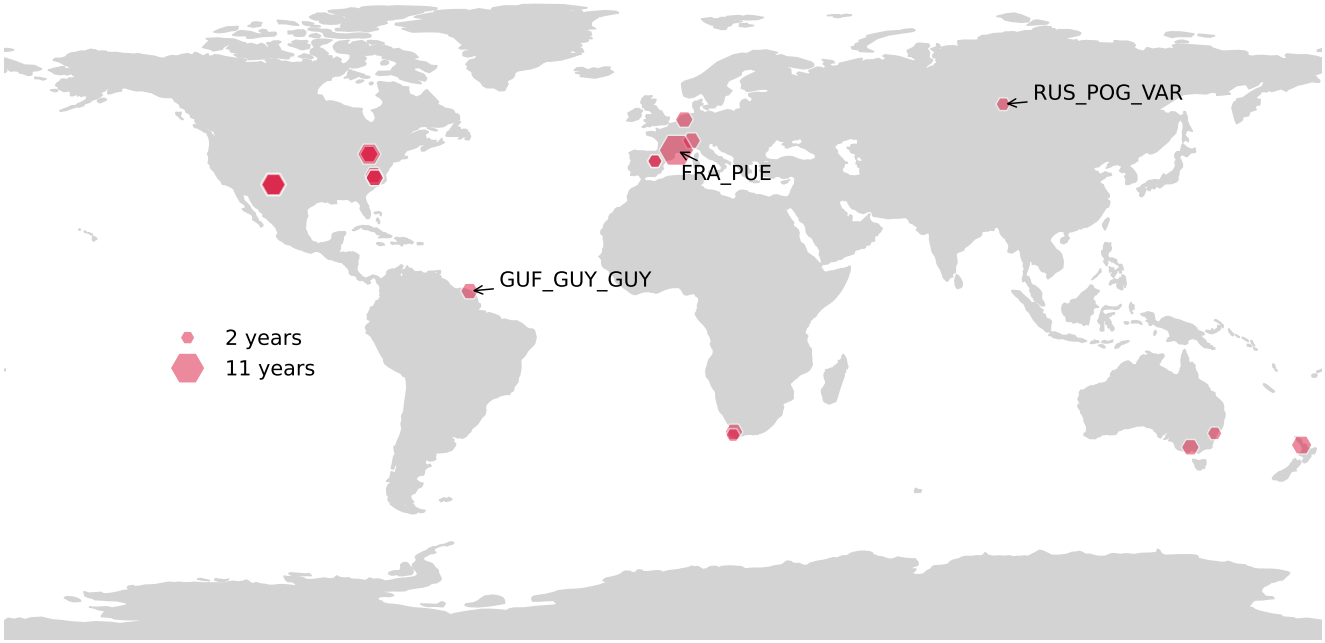

Figure 2. ~~Sites of the~~ SAPFLUXNET ~~database~~ sites where hourly SF and VPD~~(hysteresis data)~~, as well as air temperature ~~(TAir) alone, or air temperature~~ and ~~shallow~~ soil water content (SWC) have been measured at 80% of days with a length greater than 12 hours for at least 2 years. The ~~colors indicate which additional climate variables are available: gray show sites with only TAir, reddish colors show sites with TAir and SWC. The~~ size of the hexagons indicates the number of years where time series of the sap flow data and the hydrometeorological drivers overlap. ~~The annotated~~ Three sites ~~are~~ have been selected for more detailed comparison: the northernmost site ~~with valid temperature and SWC data~~ (RUS_POG_VAR), the site closest to the equator (GUF_GUY_GUY) and the site with the longest timeseries of SF and VPD (FRA_PUE).

The database includes sap flow data expressed at different levels - plant, per sapwood area, or per leaf area - which are derived from heat dissipation, heat pulse and heat balance methods (Poyatos et al., 2021). Sensors are typically inserted into the sapwood at the trunk, providing a sap flux density, i.e., the rate of flow per unit sapwood area. Plant-level data can then be calculated by multiplying this density by the total sapwood area of the tree. To obtain leaf-level data, the plant-level sap

flow is divided by the total leaf area, yielding an estimate of transpiration at the leaf scale. Not all site specific datasets include measurements for all three levels simultaneously. In this study, we selected only sites with plant-level data because it represents the largest scale of sap flow measurement, making it particularly useful for understanding whole-plant water dynamics (Poyatos et al., 2021).

In addition to sap flow (SF), the database includes observations of hydrometeorological variables such as photosynthetically active portion of incoming radiation (PAR, quantified as PPFD), 2m surface air temperature (TAir), precipitation (PRECIP), volumetric top ~~(0-30 cm)~~ soil moisture (0-30 cm, TSM) or vapour pressure deficit (VPD). With these ancillary variables, the SAPFLUXNET database allows the study of rapid tree responses to environmental conditions and helps to bridge the gap between ecosystem flux networks and remote sensing.

For the broader analysis of sub-daily sap flow dynamics and response to climatic drivers, we identified ~~33 sites~~ 15 unique sites where plant-level SF, as well as VPD, TAir and TSM are available. Specifically, we selected sites where days with these data overlapped for at least 80% of the growing season (defined based on day length > 12 hours and TAir > 5 °C) across two or more years. These ~~33 sitesrepresent less than 20~~15 sites represent less than 15% of all sites in the SAPFLUXNET database. Figure A1 shows how the mean temperature and precipitation varies across the ~~33~~ 15 study sites. Furthermore, site-level information on mean Diameter at Breast Height, Leaf Area Index, soil texture, tree species, biome, plant group, treatment and site-specific publications are provided in Tables A1 and A2.

2.1.1 ~~Case studies~~Focal sites

We selected three focal sites (highlighted in Figure 2) representing a ~~range of climates from dry Mediterranean to tropical and~~ climate gradient from tropical humid regions, to hot semi-arid, and to cold permafrost environments (see Figure A1) for a more detailed analysis. The selected sites are a mediterranean forest in Puéchabon, France (FRA_PUE), a humid tropical rainforest in French Guiana (GUF_GUY_GUY), and a forest-steppe in Pogorelsky Bor, Russia (RUS_POG_VAR). FRA_PUE was chosen for its exceptionally long time series of sap flow (SF) and vapor pressure deficit (VPD), providing a robust dataset for temporal analysis. GUF_GUY_GUY was selected as it is the site closest to the equator, representing a low-latitude humid tropical environment with a seasonal drought. RUS_POG_VAR represents the northernmost site, making it valuable for studying plant-water relations in cold, high-latitude conditions.

FRA_PUE is located 35 km northwest of Montpellier in southern France. This region is characterized by hot, sunny summers with low rainfall and strong winds, which are alternated by cool, wet winters, with rainfall primarily occurring between September and April (Limousin et al., 2009). The nearby Mediterranean Sea moderates the climate, resulting in an average temperature of 15.5 °C. However, rising temperatures due to climate change will increase drought severity in the region (Limousin et al., 2010a; Misson et al., 2011). The forest was historically managed as a coppice, meaning that all trees are approximately the same age and belong to the same species. The evergreen holm oaks (*Quercus ilex*), which reach a height of less than 7m and a diameter of less than 13cm, are situated on a plateau in a limestone karstic plateau. The soil is a shallow silty clay loam filling the cracks in the karst, with a volumetric fraction of rocks above 0.75. This leads to rapid infiltration in the subsoil and a reduced soil water holding capacity. The 25 studied holm oak trees exhibit a typical seasonal sap flow cycle,

with reduced Gross Primary Production (GPP) and transpiration during periods of drought (Limousin et al., 2009; Cicuéndez et al., 2015; ALLARD et al., 2008). This site has the longest set of measurements in the SAPFLUXNET data, spanning 15 years (2000-2015) of which we can use 2003-2015, since VPD is not available earlier.

The GUF_GUY_GUY site is located in French Guyana on the east coast of the Amazon rainforest, near the equator. The northernmost part of the Guyana Plateau is characterized by small, elliptical hills rising from 10 m to 40 m above sea level, all covered by over 400 ha of undisturbed tropical rainforest. Tropical ecosystems in this region are marked by a warm and humid climate, ~~high temperatures with~~ with Mean Annual Temperature (MAT) above 25°C and Mean Annual Precipitation (MAP) above 2500mm (Figure A1), with minimal seasonal variation, and nutrient-poor acrisol soils. The entire region experiences a dry season, most pronounced in September and October, due to changes in the Intertropical Convergence Zone (ITCZ). Despite this variability, the ecosystem maintains high transpiration rates from trees of various species, with an average height of 35 meters (Bonal et al., 2008; Aguilos et al., 2018). At this site we use data from 6 trees of mixed tropical species of varying heights from 2014 until 2016. The estimated age of the trees is 200 years.

RUS_POG_VAR is the most northerly site in the network with valid temperature and SWC data. It is located in the Krasnoyarsk forest-steppe zone in southern Russia, within the forest of Pogorelsky Bor (Urban et al., 2019). This region is characterized by extreme seasonal temperature variations and low rainfall throughout the year. Precipitation is lower during the dark winter months, when sunshine is limited. Winters tend to register sub-freezing temperatures (Figure 3). Warmer temperature in summer and increasing atmospheric water demand lead to high variation in atmospheric humidity, along with higher precipitation and transpiration rates. The soil is mainly composed of sandy loamy gray material, characterized by distinct layering, where the upper layers undergo intense leaching. (Barchenkov et al., 2023). Overall, evapotranspiration exceeds precipitation in this region (Urban et al., 2019), with ~~groundwater stored at great depths~~water stored mostly as ground water. Root-zone soil moisture is the main limiting factor for radial increment in the warm season (July-August), and can result in water stress, when surface storage is depleted (Barchenkov et al., 2023). The trees at the experimental site in Pogorelsky Bor ~~has~~ have an average age of 50 years ~~during the growing season in 2015 and 2016 and features~~ and feature a mix of six deciduous larch and three evergreen pine trees. Since larches favor wetter habitats, they respond more strongly to increased water stress and are expected to be replaced by pine species in the future(Urban et al., 2019; Tchebakova et al., 2023; Barchenkov et al., 2023). One of the key differences between the two species is their ability to regulate sap flow during periods of increased atmospheric demand, with the deciduous larches exhibiting weaker stomatal regulation under higher water stress conditions (Barchenkov et al., 2023; Tchebakova et al., 2023).

2.2 Methods

Sap flow (SF) represents the rate at which a volume of water moves through the tree per second and can be considered a proxy for transpiration and, thus, often serves as an indicator of carbon assimilation (Poyatos et al., 2016). SF has a clear diurnal cycle, driven by variations in radiation and atmospheric water demand, and regulated by plant functioning. Here, we analyse the relationship between sub-daily SF and VPD, the partial pressure deficit relative to saturated conditions, an indicator for atmospheric dryness and water demand (Figure 1). We then analyse how this relationship varies across the growing season and

over multiple years, and how it relates to other environmental variables, including temperature, soil moisture and radiation, as described below.

For each of the ~~33~~ 15 sites, we aggregated half-hourly VPD and average SF data across all measured trees into hourly values per site. Since some sites only provided hourly data, this step ensured consistency across sites. We then analyse the diurnal cycle of paired SF–VPD values~~, as shown in Figure 3 (left column)~~. As discussed in the introduction, we hypothesise that the sub-daily dynamics can be used to understand plant stress, and derive two metrics at a daily basis to characterize the diurnal SF–VPD relationship~~, illustrated in Figure 3 (left column)~~: the magnitude of the morning slope of the ~~curve (SLOPE)~~ SF–VPD curve, referred to as SLOPE, and the area of the ~~curve (AREA)~~hysteresis loop (Zuecco et al., 2016), referred to as AREA. Other metrics were tested in preliminary analysis, such as the magnitude of the afternoon SF–VPD slope, or the temporal lags between peak SF and peak VPD (analogous to e.g., Wan et al. (2023)), but we found the information in these metrics to be strongly correlated, and thus redundant, with the two presented here.

The SLOPE is calculated as the coefficient from a linear regression of VPD and SF between the times of minimum VPD and maximum SF. AREA corresponds to the area enclosed by the hysteresis curve of SF and VPD during the diurnal cycle, measured as the area of a polygon formed by the observation points. The variable SLOPE shows outliers (upper 5 %) and sometimes negative values, particularly when VPD gradients throughout the day are too small, e.g., in winter. These values were excluded from the analysis, resulting in a filtered SLOPE. In order to make the values comparable across sites, we standardize the filtered SLOPE values with the median and scale the AREA to 0–1 per site. These quantities are indicated as sSLOPE and ~~sAREA~~nAREA.

We analyse the seasonal variability of the two metrics for the selected sites along with the seasonal changes in PPFD used as a measure of solar radiation, TAir ~~andTSM~~ and TSM for the three focal sites. For this, we first evaluate the seasonal cycle of each variable per site ~~(Figures 3)~~ and in a second step correlate the seasonal cylces of SLOPE and AREA to each of the hydrometeorological drivers~~, as shown in Figures 4, ??~~. To reduce redundancy, when a site was represented by multiple plots, we averaged the correlation coefficients and p-values across plots to obtain a single site-level estimate.

Since we want to evaluate plant functioning and water fluxes under environmental stress, we analyse combined extremes of TAir and TSM (upper and lower 20 % of ~~the data~~all days within the growing season at each site). We obtain the following four extreme conditions: cold & wet, hot & wet, hot & dry and cold & dry. ~~If one of these clusters has less than eight samples, we discard it from the further analysis.~~ Within each of the remaining clusters, we calculate the values of sSLOPE and ~~sAREA~~ nAREA and the hysteresis of the mean diurnal cycle~~(Figure 5).~~ . In order to get a more general picture of diurnal hysteresis during extreme conditions, we evaluated the metrics at all 15 sites (Figure 6). In order to make the sites comparable, we evaluated sSLOPE and nAREA at anomalies of TAir and TSM (upper and lower 20 %, after subtraction of the mean).

Finally, to evaluate the feasibility of large-scale monitoring of plant stress, for example, through remote sensing of VWC (see ~~1~~Figure 1), we investigate how these two sub-daily metrics depend on the temporal resolution of the sub-daily observations. For this, we tested four scenarios of sub-daily sampling: 3-hourly, starting at mid-night (8 times per day, 8TPD), 6-hourly, starting at mid-night (4TPD) and 6-hourly with mid-night or noon left out (3TPDday, 3TPDnight). We then derived the curves of SF–VPD at the coarser temporal resolution ~~(Figure 7)~~ and calculated the corresponding sub-daily metrics. To evaluate whether

the metrics could still be reliably estimated at coarser temporal resolution, we determined the corresponding coefficients of determination (Pearson R^2) between the metrics derived from the resampled time series and the metrics derived from the hourly data for the complete data record at each site.

3 Results

3.1 Sub-daily and seasonal dynamcis of SF–VPD and hydrometeorological drivers

3.1.1 Seasonality of sub-daily hysteresis captured by daily metrics

The mean diurnal cycle of the bivariate relationship between SF and VPD for each ~~site is shown in Figure 3 (left column), together with the corresponding metrics, AREA and SLOPE. We find that the diurnal hysteresis, characterised by the AREA of the hysteresis curves, and the morning sensitivity of SF to VPD vary over the course of the year at all sites, as vegetation responds to the evolving hydrometeorological conditions. This is illustrated by the seasonal cycles of daily values of SLOPE and AREA and the climate drivers (PPFD, TSM, TAir: Figure 3, right column) for each of the~~ of the focal sites (FRA_PUE, GUF_GUY_GUY, RUS_POG_VAR) is shown in Figure 3 (a, c, e), together with the mean seasonal cycles of the two metrics derived from these diurnal hysteresis curves (AREA and SLOPE), shown in Figure 3 (b, d, f). Note that the two metrics based on the diurnal SF-VPD cycles have daily time steps.

~~First we discuss the diurnal dynamics of SF and VPD relationships (Figure 3, left panel)across sites. Generally,~~ On average, hourly SF and VPD show very low (close to zero) values during night-time, with SF increasing as VPD increases through the morning. SF peaks around peak VPD for the three sites, before declining through the afternoon into the evening, in response to decreasing VPD. ~~Hysteresis is therefore characterized by lower SF rates in the afternoon compared to periods in the morning with comparable values of VPD (son; Zheng et al., 2014) as a consequence of a change in the velocity of the SF response to atmospheric demand in the either morning or afternoon or both.~~ The absolute rates of SF, as well as the peak times of SF and VPD vary across sites~~, as does~~. As a result, the degree of hysteresis in ~~a typical cycle , reflecting differences in hydraulic supply and transport across vegetation types and site conditions. To explore potential links between the metrics and climatic drivers associated with plant stress, we examine the average seasonal cycles of daily values characterizing the diurnal cycle. Their correlations are discussed in Section 3.1.2.~~ an average diurnal cycle and the slope of the curve in the morning (represented by the blue lines) also differs across sites, which we discuss individually below.

At FRA_PUE (~~upper panel~~ panel a and b), the average diurnal cycle shows ~~strong hysteresis with the peak SF~~ peak SF occurring around solar noon before ~~the peak VPD~~peak VPD, which occurs around 2pm ~~. On average, the morning SF is aligned~~ on average. The morning SF aligns closely with rising VPD, ~~which is captured~~ with the rate of SF increase per unit of VPD increase in this period reflected by SLOPE. The rate of increase of SF with VPD begins to drop off ~~late in the morning (~~in the late morning (after 10am), and remains depressed relative to decreasing VPD throughout the afternoon, leading to a characteristic hysteresis loop, whose aperture is captured by the AREA. ~~The seasonal cycle of the morning SLOPE closely tracks the temporal evolution of TSM (Pearson's correlation, R = 0.60). In April, SLOPE values are are approx. 0.5~~

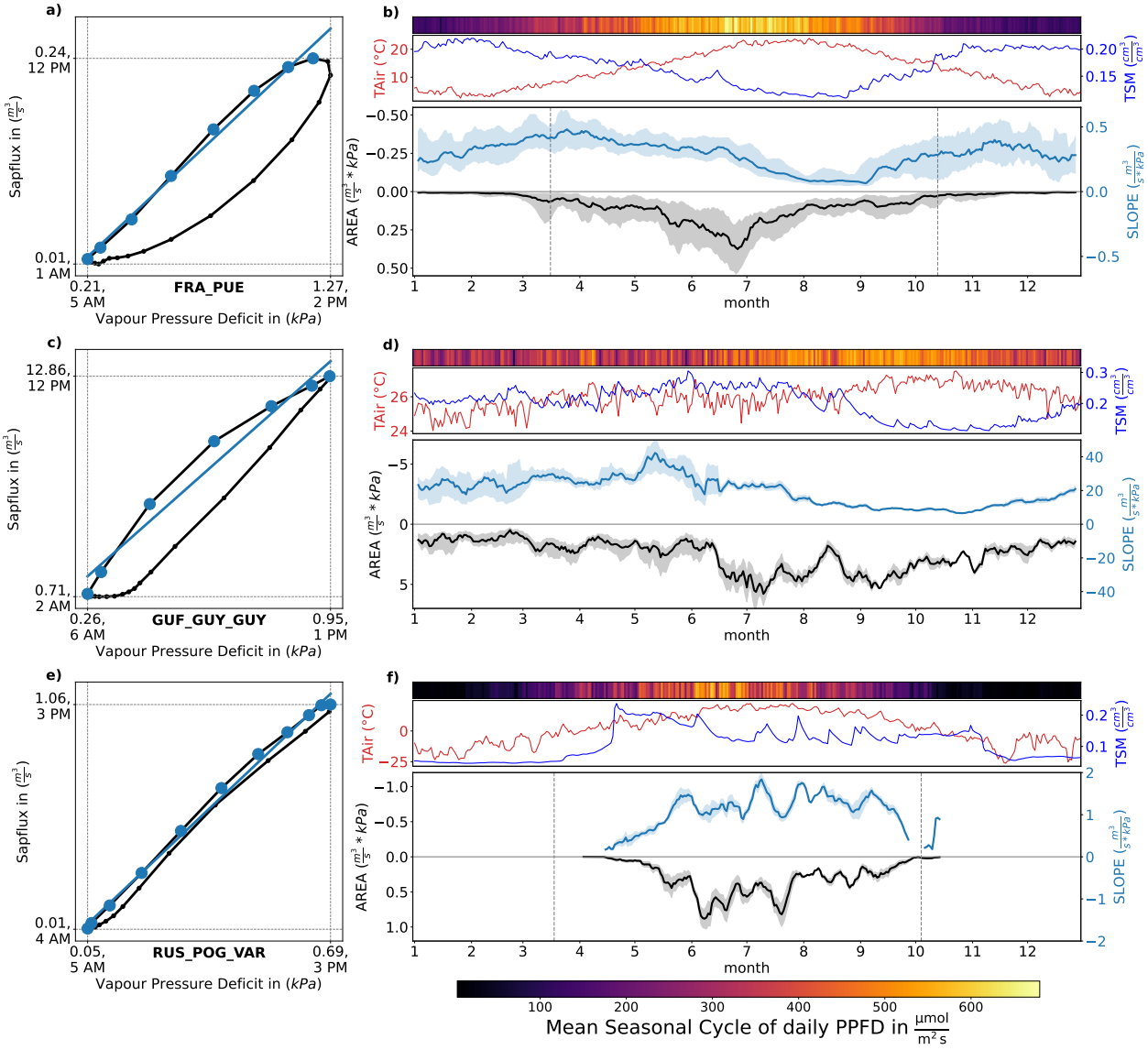

Figure 3. ~~Left column~~Illustration of metrics derived from diurnal SF-VPD relationships and their variability across seasons. a), c), e): Illustration of the approach used to calculate the ~~sub-daily~~ two metrics used in this study, based on the mean diurnal cycle of ~~sub-daily~~ hourly VPD and SF measurements, aggregated over all trees and all days for the whole time span of available data for three selected sites: FRA_PUE, GUF_GUY_GUY, RUS_POG_VAR. The morning slope (SLOPE) is calculated through a linear regression of all ~~points~~ hours (colored blue) between minimum VPD and maximum SF, while the area (AREA) is the area ~~within the polygon obtained~~ enclosed by ~~linking~~ connecting the data points ~~at~~ for all available ~~sub-daily timesteps~~hourly timestamps. ~~Right column~~The dashed vertical and horizontal lines indicate the maximum values of the mean seasonal cycles of VPD and SF, and the corresponding average time of the day. b), d), f): Seasonal dynamics of daily values of photosynthetically active ~~portion of incoming~~ radiation (PAR, quantified as daily PPFD), air temperature (TAir) and top soil moisture (TSM), AREA and SLOPE with interquartile ranges showing the range of the hydrometeorological drivers and the derived metrics per day across years. The vertical lines indicate the selected growing season, i.e. when the ~~daylength~~ day length is higher than 12 hours and temperature > 5 °C. Absolute values of SLOPE vary according to the magnitude of tree-specific SF rates.

~~$m^3/(s \cdot kPa)$, decreasing slowly through late Spring and more abruptly with the decline in available soil moisture during the summer months, where morning slopes close to 0 $m^3/(s \cdot kPa)$ indicate strongly limited hydraulic transport. SLOPE gradually recovers through the Autumn as TSM recharges. In contrast, the AREAvalues follow more closely the seasonality of PPFD (R = 0.84), peaking in June, before declining as water limitation suppresses the SLOPE of the morning limb of the hysteresis curve. The interannual variability in SLOPE and AREA, given by the spread around the mean values, is generally greatest outside the core of the dry season.~~

Similarly to FRA_PUE, the average diurnal cycle also shows a hysteresis at GUF_GUY_GUY (~~mid panel~~ panel c and d), but here, hysteresis appears to emerge as a result of stomatal restrictions on SF initiating earlier in the morning (breakpoint at 9am). Timings of peak SF and VPD align at 12pm and the afternoon SF is aligned with VPD, with a strong stagnation at night close to minimum SF until SF starts to rise again in the morning. Despite these differences, the morning slope of the hysteresis curve similarly responds to changes in ~~top soil moisture (R = 0.68)~~TSM, with slopes of 20-40 $m^3/(s \cdot kPa)$ during the wettest part of the year (January-July), decreasing to a minimum of approx. 8 $m^3/(s \cdot kPa)$ in November, when soils are driest. AREA is closely related to PPFD~~(R = 0.64)~~, but as observed at FRA_PUE, AREA starts to decrease in the driest parts of the year when SLOPE is suppressed by lower ~~soil moisture.~~

TSM values. In contrast, at RUS_POG_VAR (panel e and f), the average diurnal cycle of SF is aligned with the diurnal cycle of VPD with very little hysteresis (lower left panel), with ~~peaks~~ maxima of both variables at 3pm and minima at ~~night.~~ ~~Variations in the AREA of the diurnal hysteresis curvethrough the growing season(May/June-September) are also strongly and positively correlated with temperature (R = 0.71) and PPFD (R = 0.66). However, SLOPE is variable throughout this period, and less closely correlated with soil moisture than at other sites (R = -0.14). Instead SLOPE is related to temperature in the cold climate (R = 0.46), similar to AREA.~~ 5am and 4am, respectively.

The daily values of SLOPE and AREA derived from diurnal SF–VPD curves also show distinct seasonal variability patterns. In FRA_PUE, SLOPE values vary from approx. 0.2–0.5 $m^3/(s \cdot kPa)$ during January to April, decreasing slowly through late spring and more abruptly with the decline in TSM during the summer months, where SLOPE values close to 0 $m^3/(s \cdot kPa)$ indicate strongly limited hydraulic transport. SLOPE gradually recovers in autumn as TSM recharges. In contrast, AREA values follow more closely the seasonality of PPFD , peaking in June, before declining as water limitation suppresses the SLOPE of the morning limb of the hysteresis curve. The interannual variability in SLOPE and AREA, given by the spread around the mean values, is generally greatest outside the core of the dry season.

In GUF_GUY_GUY, SLOPE remains constant at about 20-40 $m^3/(s \cdot kPa)$ during the wet season (January-July), decreasing over the dry season to a minimum of approx. 8 $m^3/(s \cdot kPa)$ in November, when soils are driest. AREA shows less marked seasonality than the other two sites, but with a peak right before the start of the dry season around mid-July to August, and remaining high throughout the dry season (late July to November). At RUS_POG_VAR, AREA shows an increase at the onset of the growing season (May to June), but then showing variability throughout summer months, and followed by a fast decline from August onward. Contrary to FRA_PUE, SLOPE increases markedly at the start of the growing season and remains high, with strong sub-seasonal variations, until around September, when it decreases sharply.

3.1.2 Relation of SLOPE and AREA to climate drivers

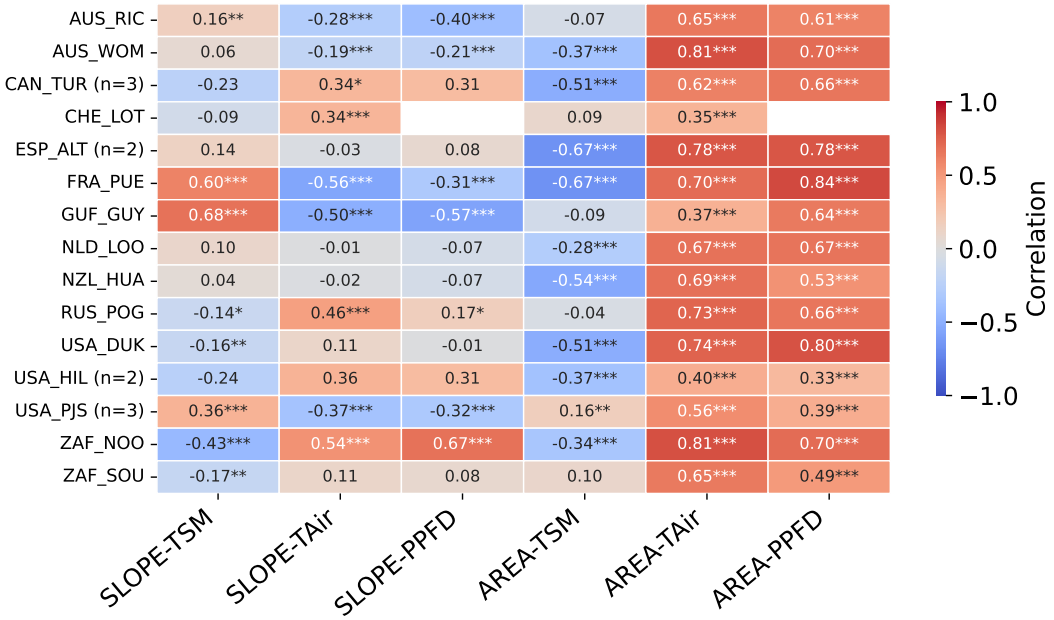

Figure 4. Heatmap of Pearson's correlation coefficients of the ~~seasonal cycles~~ daily values of the ~~metrics~~ SLOPE and AREA metrics and of hydrometeorological drivers (TSM, TAir and PPFD) ~~. Results are shown for each of~~ over the ~~focal sites individually and the results for~~ growing season across all studied sites. ~~Maps~~ The number of ~~coefficients~~ plots at ~~all~~ sites ~~are provided in Supplementary Materials (Figure ??)~~with multiple plots is indicated by n. Asterisks denote statistical significance, with three asterisks indicating $p < 0.001$, two indicating $p < 0.01$, and one indicating $p < 0.05$.

~~We~~ Here, we analyse the relationship of SLOPE and AREA metrics and hydrometeorological drivers ~~(~~through the correlation of daily mean values of TAir, PPFD, and TSM ~~) through the correlation of daily values at the three selected~~ and the daily values of the AREA and SLOPE over the growing season for the broader selection of fifteen SAPFLUXNET sites, shown in Figure 4~~and across all sites (Figure ??).~~.

~~For the three selected sites, both FRA_PUE and RUS_POG_VAR show strong and comparable in magnitude correlations between AREA and TAir and AREA and PPFD. At the tropical site~~ Across all 15 sites, AREA correlates positively and with comparable magnitude with TAir and PPFD (Figures 4), while AREA and TSM tend to correlated negatively, with larger variations across sites. For the focal sites, GUF_GUY_GUY ~~AREA~~ shows a much weaker relationship ~~with~~ between AREA and temperature (R=0.37~~) than with~~ , Pearson correlation) than AREA and PPFD (R=0.64)~~. At the Russian site, the positive correlation of AREA with PPFD (R=0.66) and TAir (R=0.71) is much stronger than any other pair at this site, indicating that the hysteresis is more strongly connected to atmospheric drivers than soil characterisitics~~, while FRA_PUE shows the strongest correlation between AREA and PPFD across all sites.

The relationship of SLOPE with hydrometeorological drivers varies more across sites than for AREA. In general, the tropical and Mediterranean sites show similar patterns, with increasing SLOPE associated with increasing TSM (correlation values higher or equal to 0.6), but with three groups that can be distinguished. A first group of five sites (AUS_RIC, AUS_WOM, FRA_PUE, GUF_GUY and USA_PJS), shows predominantly positive correlations between SLOPE and TSM (R=0.16–0.68), and negative correlations of SLOPE with TAir (R=-0.56– -0.19) and decreasing SLOPE with increasing TAir and PPFD (correlations lower than -0.31). In contrast, the Russian site exhibits an inverted pattern, which results in both metrics responding in the same direction to the drivers. The observation, that SLOPE decreases with higher TSM is contradictory and will be discussed later. However, the coefficients at this site are generally less strong. At FRA_PUE, the negative relation of SLOPE to PPFD (-0.31) is almost half of its relation to temperature (-0.56)

Comparing the R=-0.57– -0.21), while another group of seven sites (CAN_TUR, CHE_LOT, USA_HIL, USA_DUK, ZAF_NOO, ZAF_SOU, RUS_POG_VAR) shows the opposite pattern: negative correlations of SLOPE and AREA across the global collection of sites (Nwith TSM (R=33, 4 ("all") , **??**) highlights considerable variability in relationships between sub-daily hysteresis characteristics and environmental drivers. AREA is generally positively associated -0.43– -0.16, not significant for CAN_TUR) and positive or no relationship with TAir and PPFD (mean Rvalues of 0.60 and 0.61 across all sites, respectively), and negatively associated with TSM (mean R=-0.24), although the strength of these correlation varies across sites (Figure **??**). For most sites , no clear pattern emerges by latitude, though there may be a climate-related pattern. The relationship 0.46–0.54 and R=0.17–0.67, for significant values only). The remaining sites show no significant correlation between SLOPE and environmental drivers is less consistent across the global network of sites, resulting in very low average correlation values (Figure 4), although sites with a positive correlation of the metrics to TAir and PPFD exhibit a negative correlation to TSM, and vice versa (Figure **??**). Interestingly, some sites show a close-to-zero relation of SLOPE to all three drivers, namely TSM, PPFD, and TAir. any of the three hydrometeorological variables. These differences appear to be associated with hydrometeorological regimes, with the first group predominantly associated with sites with marked dry seasons and the second group corresponding to cold/temperate sites, or sites in semi-arid regions but where irrigation is practiced (Table A2).

3.2 Diurnal SF–VPD dynamics during extreme conditions

Upper row: Scatterplots of absolute TAir vs. TSM values for each focal site. Extreme percentile clusters (upper and lower 20 % of TAir and TSM) are colored by sSLOPE and scaled by sAREA; clusters with fewer than eight samples are not shown. Lower row: Diurnal cycles of SF (y-axis) vs. VPD (x-axis) for the identified clusters, with SLOPE shown in blue and AREA indicated by black circles with different linestyles for the hydrometeorological regimes: hot&wet (solid), hot&dry (dotted), cold&dry (dashdotted), cold&wet (dashed).

To Next, we compare diurnal SF–VPD dynamics under varying climatic conditions, we cluster days according to extreme percentiles of temperature and top soil moistureand the associated AREA and SLOPE values under varying hydrometeorological conditions, classified according to combinations of upper and lower 20% percentiles of TAir and TSM (Figure 5, and see Section 2.2). This procedure yields four clusters (of moderate to extreme cold & wet, hot & wet, hot & dry and cold & dry),

~~although not all are present at all sites since we discard clusters with fewer than eight samples.~~ conditions. The clusters and their corresponding mean diurnal cycles of absolute SF-VPD are ~~shown~~ illustrated for the three focal sites in Figure 5. Given that we selected the three sites based on their different climate zones, the values of ~~Tair~~ TAir and TSM differ strongly in their absolute ranges for the different clusters as does absolute SF, given the differences in evaporative demand, but also differences in DBH and leaf area index (Table A1). Nevertheless, this ~~allows~~ clustering approach allows us to compare relative ~~extremes in hydrometeorological drivers, and the corresponding response of SF to VPD.~~ responses of SF-VPD dynamics to different to hydrometeorological conditions and evaluate how the SLOPE and AREA metrics reflect these responses.

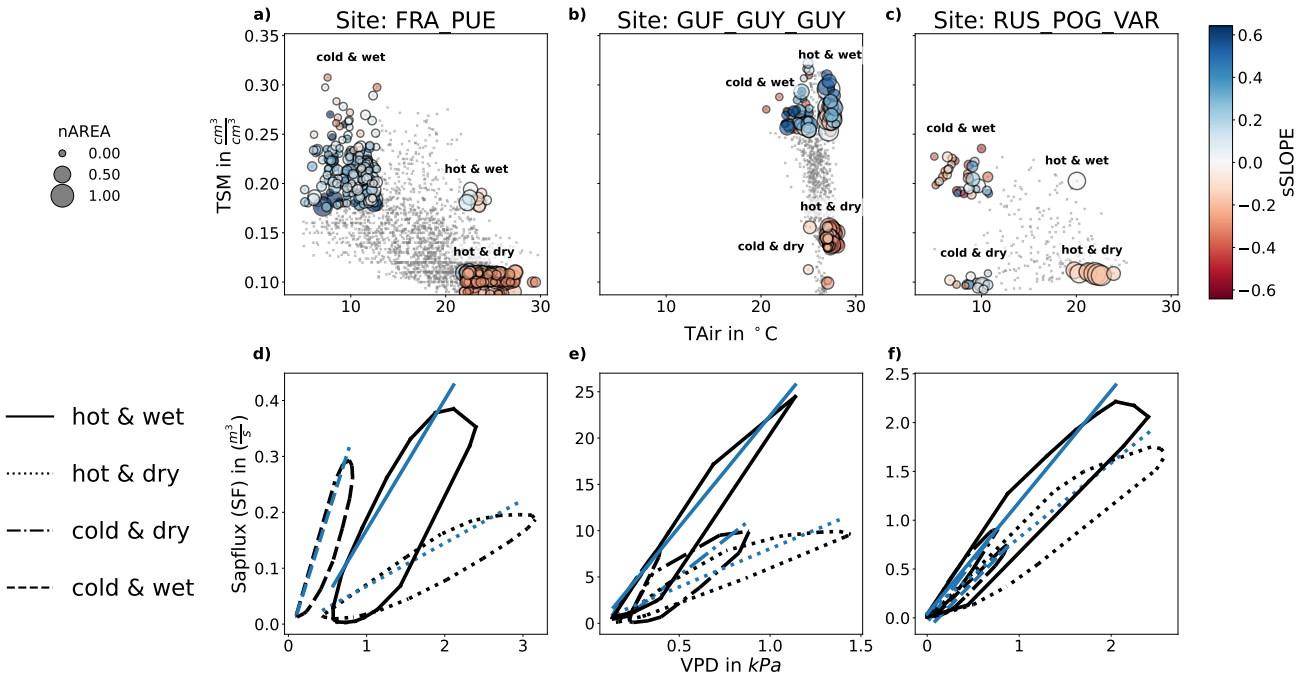

Figure 5. Changes in the SF–VPD diurnal cycles in response to varying hydrometeorological conditions. a)-c): daily mean values of absolute TAir and TSM for each focal site (upper panel) and the four clusters corresponding to different combinations of the upper and lower 20% percentiles of daily mean TAir and TSM. The markers are colored by the corresponding values of sSLOPE and scaled by sAREAd)-f): Mean diurnal cycles of hourly VPD (x-axis) vs. SF (y-axis) for each of the focal sites, and for the four clusters corresponding to different hydrometeorological regimes: hot&wet (black solid line), hot&dry (black dotted line), cold&dry (black dash-dotted line), cold&wet (black dashed line). The corresponding SLOPE is shown in blue for each of the four curves, per site.

Across the three focal sites, and despite their different background climate, sub-daily dynamics exhibits similar responses to ~~local hydrometeorological extremes~~ the different hydrometeorological clusters (Figure 5). Hot days, ~~associated with~~ generally reaching higher VPD values, are ~~generally~~ characterized by higher ~~AREA values~~ hysteresis (and thus higher AREA values) than cold days at all three sites. ~~Hot and dry~~ However, hot and wet days tend to be associated with ~~a reduction in the~~ steeper morning and afternoon slopes compared to hot and dry days,with the latter associated with a lower morning SLOPE, ~~indicating~~

~~suppression of transpiration driven water loss, even under very high VPD,~~ which is indicative of suppression of SF when soil moisture is most likely to be a limiting factor, even under very high VPD.

~~Site-specific responses refine this general picture, even if absolute values of SLOPE vary across sites due to the magnitude of SF~~Despite these similarities, we also note differences between the three sites (Figure 5). FRA_PUE shows the clearest separation between hydrometeorological regimes (panel a and d): cold–wet days ~~combine low~~ are associated with low values of AREA with high SLOPE values, hot–wet days show high AREA values with reduced SLOPE and the highest peak SF, and hot–dry days reveal negative SLOPE anomalies with lower AREA than hot–wet days but still higher than cold–wet days. At this site, nighttime VPD minima do not return to zero ~~under hot conditions~~in hot days, although SF can still cease. GUF_GUY_GUY ~~show distinct~~ (panel b and e) also shows contrasting dynamics for high- and low-TSM regimes, although it is worth noting that dry days are still considerably wetter than dry days in FRA_PUE and RUS_POG_VAR. SLOPE ~~remains similar across~~ is higher for the wet regimes ~~, but AREA increases~~ than dry ones, while AREA is higher in hot days ~~, though~~ than cold days, although the difference of hot versus cold is only $5\,^{\circ}\mathrm{C}$ at this site. At ~~hot-dry~~ hot-wet days, peak SF exceeds all other regimes by more than a factor of two. In RUS_POG_VAR ~~, in contrast,~~ (panel c and f), hot conditions are associated with higher AREA and dry days are associated with lower SLOPE, although the variability observed in SF–VPD ~~dynamics separates mainly by temperature. An optimal range begins at about $8\,^{\circ}\mathrm{C}$, with high AREA occurring only at the warm end. Peak SF is reached on hot–dry days , whereas cold days show tight alignment between SF and VPD. On hot–dry days, SF stagnates slightly at mid-day but SLOPE remains high, a clear contrast to the warmer sites.~~ hysteresis between relative hydrometeorological extremes at this site is less marked than at FRA_PUE and GUF_GUY_GUY.

~~Finally, we find specific breakpoint of the average diurnal cycle per cluster, which highlight the diversity of site responses (Figure 5).~~

~~Breakpoints in the diurnal SF—VPD relationship mark the onset of stomatal regulation, when atmospheric water demand through VPD keeps increasing, but SF increase slows down, or SF remains constant or even decreases. FRA_PUE exhibits inverting breakpoints during hot–wet days, consistent with onset of strong stomatal regulation during the morning before VPD reaches its maximum early in the afternoon. GUF_GUY_GUY also shows a morning breakpoint for hot-wet days , but SF increases at a slower rate with increasing VPD, rather than inverting. The hot-wet regime generally occurs only rarely in RUS_POG_VAR, underscoring the climatic constraints of this energy-limited site.~~

~~In hot-dry days all 3 sites show a morning breakpoint, which is followed by a stagnation of SF under increasing VPD for both FRA_PUE and GUF_GUY_GUY, and a slow-down of the SF increase in RUS_POG_VAR. Together with a typical stagnation to nearly constant nighttime SF during hot –wet days at the warmer sites in this regime, this increases AREA of the hysteresis curve. Both FRA_PUE and GUF_GUY_GUY feature afternoon breakpoints at similar or lower VPD thresholds compared to the morning breakpoints, especially for hot-wet conditions.~~

~~Cold conditions tend to be associated with smaller VPD ranges and lower hysteresis across the three sites, with a breakpoint in peak SF very close to peak VPD for both cold-wet and col-dry conditions. In FRA_PUE and GUF_GUY_GUY, cold and wet conditions show the highest value of morning slope. The cold-dry extremes are only found at RUS_POG_VAR, where~~

~~SF–VPD curves exhibit small hysteresis. This regime occurs at the very start and end of the growing season, where overnight temperatures are likely to be below freezing, and there are potential interactions between hydraulic transport, snow and frost.~~

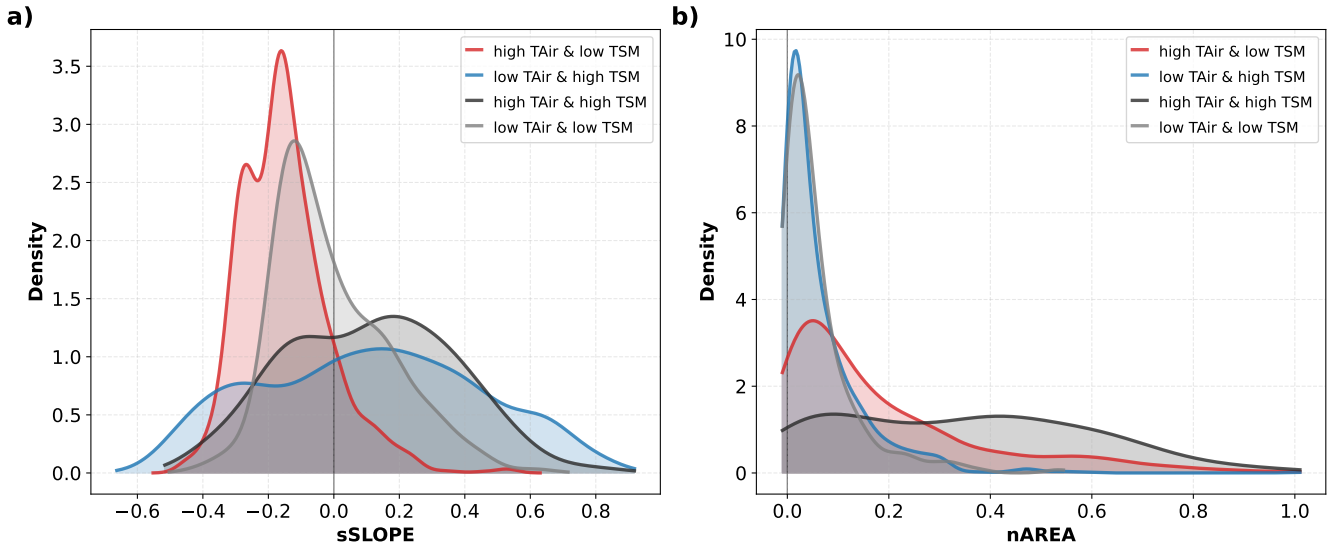

Figure 6. Distribution of a) sSLOPE and b) nAREA at extreme anomalies of TAir and TSM for all 15 sites for different groups of hydrometeorological extremes, as shown in Figure 5 for the three representative sites. Red curves correspond to hot and dry days (high TAir and low TSM), blue curves to cool and wet days (low Tair and high TSM), black curves to hot and wet days (high TAir and high TSM) and grey curves to cool and dry days (low TAir and low TSM).

Based on these results, the AREA and SLOPE descriptions appear to reflect characteristic hydrometeorological regimes across the three focal sites, allowing to distinguish distinct types of responses to environmental stressors. To evaluate whether these differences can be generalized across sites, we analyse the distributions of sSLOPE and nAREA at all 15 sites during the four types of hydrometeorological regimes (Figure 6).

For the standardized SLOPE (sSLOPE, panel a), distributions show significant differences between wet and dry hydrometeorological regimes: for both cold and hot days with high TSM, the distributions of sSLOPE show a large spread with positive median values ($median = 0.12$), while for days with low TSM, the distributions are strongly skewed towards negative sSLOPE values, with median values of -0.16 and -0.05 for hot and dry and cold and dry days, respectively.

In the case of the normalized values of AREA (nAREA, panel b), we find stronger differences in the between hot and cold hydrometeorological regimes: cold days show a predominance of very small values, and very similar distributions for cold days whether the soil is wet or dry, with comparable median values (0.03) and a similar tail distribution. By contrast, hot days show very long tails and median values shifted towards higher values (0.11 and 0.35 respectively), which is particularly pronounced for the regime corresponding to hot conditions and high TSM.

3.3 Dependence of sub-daily metrics on sampling rate

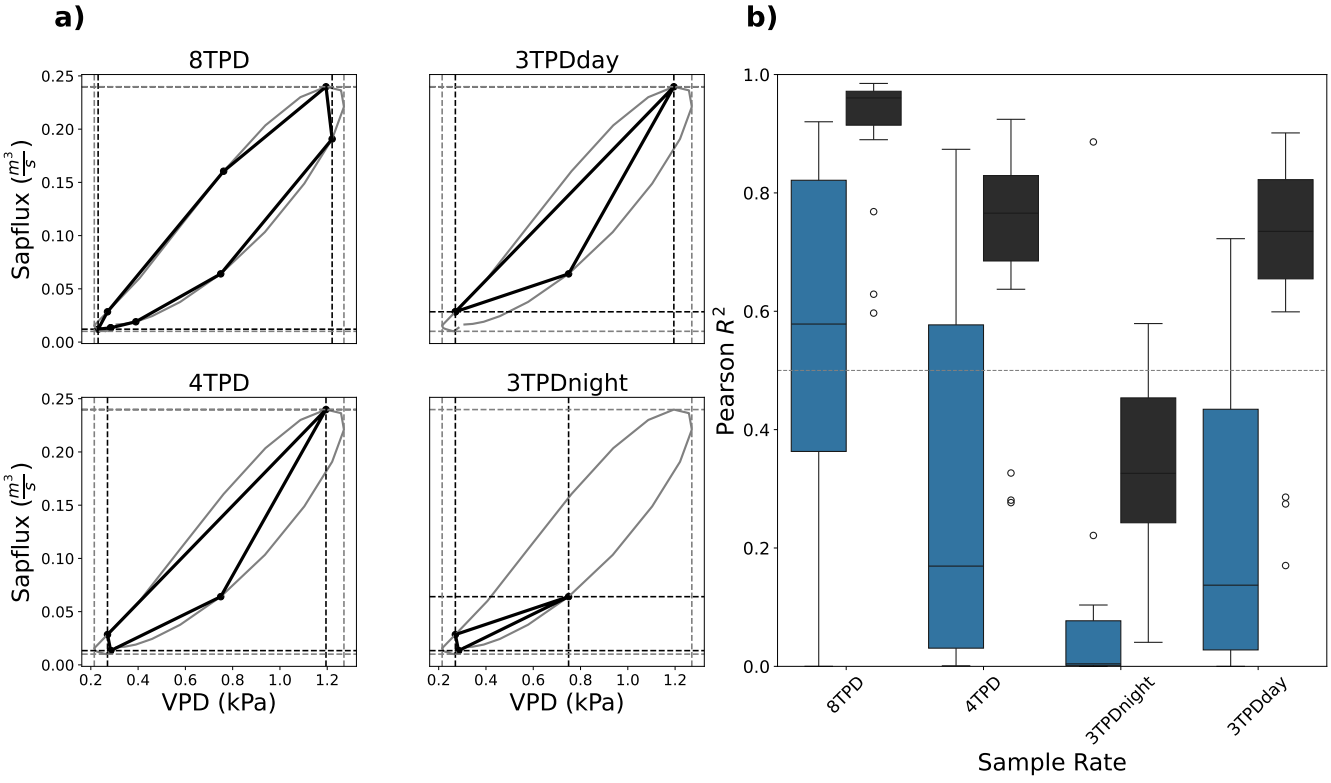

Figure 7. ~~A) Diurnal cycle (average across days~~ Effect of temporal resolution and ~~trees~~sampling times on the two diurnal cycle metrics. a): illustration of ~~measurements in~~ the average diurnal cycle for FRA_PUE, estimated based on hourly measurement (solid gray lines), and the corresponding diurnal cycle captured by measurements at different sample rates ~~:~~ (bold black lines). The vertices of the ~~gray cycle in~~ curves under lower sampling rates indicate the ~~background of each subplot represents hourly~~ observations ~~. The black overlaid polygons show observations~~ at ~~four~~ different ~~sample~~ sampling rates: 3-hourly, ~~which are used to calculate~~ starting at mid-night (8 times per day, 8TPD), 6-hourly, starting at mid-night (4TPD) and 6-hourly with mid-night or noon left out (3TPDday, 3TPDnight). The vertical and horizontal dashed lines indicate the ~~metrics from these lower sample rates~~corresponding maximum values of the reference diurnal cycle with hourly time steps (gray) and with coarser temporal sampling (black). ~~B~~b): Boxplots of coefficients of determination (R^2) estimated as the relationship between daily time series of the AREA (black) and SLOPE (blue) metrics at different sample rates (x-axis) and the ~~hourly~~ reference values derived from hourly sampling. ~~One R^2 was calculated per site for the whole period of available data, so the distributions~~ The boxplots summarize the variability of ~~correlations~~ R^2 across all sites ~~. These values mainly~~ and reflect how closely the seasonal dynamics of the metrics ~~from~~ based on resampled time series ~~of SF and VPD~~ track those of the hourly reference across sites~~, shown for AREA (black) and SLOPE (blue)~~.

~~The analysis thus far has been based on sap flow, continuous observations of which can be obtained from in-situ sensors. The fine temporal resolution ensures that the diurnal cycle is well-captured and the SLOPE and AREA can be calculated with~~

some accuracy. However, what if fewer data are available? The limitation of sap flow data is that they are available only for few sites, and covering relatively short periods. Other datasets, for example, from remote sensing could in principle address this limitation and provide global coverage, but trade-offs in temporal resolution usually need to be considered.

While in situ sensors can provide continuous sap flow data, we consider the potential to estimate these descriptors of the diurnal cycle using temporally sparse data (see Sections 1 and 2.2). In particular, as sap flow is connected to changes in water storage, which can be estimated using microwave remote sensing, we examine the degree to which the SLOPE and AREA can be estimated for several acquisition strategies with different numbers of observations and acquisition times. To determine optimal measurement frequency in order to derive the two metrics discussed above, e.g. using remote-sensing observations or more temporally sparse measurements, we analyzed the

Figure 7b) shows the distribution of the coefficients of determination for the metrics AREA and SLOPE across varying sampling frequencies for the longterm period of (Pearson R^2) obtained by linear correlation of the daily values of the SLOPE and AREA metrics derived from the hourly data, and those derived from sparser sub-daily sampling frequencies and the values for each site. We tested frequencies ranging from 8 (3-hourly), 4 (6-hourly), and 3 (6-hourly with either mid-night or mid-day left out) times per day (TPD) starting at 6am, as illustrated in Figure 7 (left panel panel a) for FRA_PUE. Each box summarizes the distribution of coefficients of determination obtained from correlating the daily values of the two variables for each of the 33 sites, thus reflecting the overall variability and strength across the 33 sites.

The synchronization of resampled and hourly AREA is generally well preserved across sampling strategies, particularly at higher temporal resolution, and declining performance at reduced sample ratesThe AREA descriptor calculated with coarser temporal sampling agrees well with the AREA estimated using hourly data, though the agreement obviously declines when fewer data are used in the estimation. With 8TPD, the metrics AREA values are well preservedacross all years, with a median annual coefficient of determination of Pearson R^2 of 0.95 and an interquartile range of 0.9–0.97. For 4TPD, the relationships between the metrics AREA values derived from sparse sampling and the higher temporal resolution become weaker and less well constrained, as given by the median correlation of 0.76 and interquartile range of 0.67–0.83. Sampling There is very little further information loss in AREA estimation when sampling at 3TPD results in further degradation, with median values of R2 of 0.3 and when there is an observation at noon (3TPDday, median R^2: 0.74; IQR: 0.66–0.83). However, there is significant degradation in the relationship for 3TPDnightand 3TPDday, respectively, and corresponding interquartile ranges of , where the observation at noon is missing (median R^2: 0.30; IQR: 0.22–0.45and 0.66–0.83.)

Compared to AREA, the estimates of SLOPE are more sensitive to sampling frequency and exhibit greater variability across the sites, especially at 8TPD. At 8TPD, the correlation with the hourly sampling shows a median value of 0.5 with interquartile range of 0.26–0.82. Similarly to the performance of AREA, the agreement of SLOPE calculated with lower sampling rates deteriorates with decreasing frequency: with median correlations of 0.16, 0.01 and 0.14 for 4TPD, 3TPDnight and 3TPDday, respectively. Also Furthermore, the correlations of SLOPE show large variability across sites for 4TPD and 3TPDday show large spread, with interquartile ranges of 0.03–0.55 and 0.02–0.37, respectively. In general, AREA is underestimated at lower sampling frequencies.

The diurnal cycles of SF–VPD under sparse sampling, shown in ~~the left panel of Figure 7~~Figure 7a), illustrate the poor performance of 3TPDnight in estimating SLOPE at least for FRA_PUE. 3TPDnight cannot accurately capture maximum SF (see Figure 7~~, left~~a), even though it does effectively capture minimum VPD. In contrast, 4TPD and 3TPDday slightly overestimate minimum VPD but still yield better SLOPE estimates, with 3TPDday performing best among the reduced sample rates. ~~In general, AREA is underestimated at lower sampling frequencies. Likewise,~~

With the sample times considered, maximum VPD tends to be underestimated~~across all sample rates~~, reducing accuracy in metrics relying on its diurnal extremes at this site. ~~At other sites the peak times of SF and VPD and the general evolution of the diurnal cycle differ from FRA_PUE, potentially leading to different best sample rates . Nevertheless the samplerates~~ Nevertheless the sample rates of 4TPD and 3TPDday still capture the metrics similarly at all sites, with better results of AREA at 4TPD and better results for SLOPE at 3TPDday.

4 Discussion

4.1 Metrics as indicators for tree stress

~~The diurnal cycle of SF and VPD provides diagnostic indicators that consistently discriminate the drivers of extreme stress across three contrasting forested sites.~~ Sap flow (SF) alone is not a reliable ~~stress indicator~~ indicator of vegetation response to environmental conditions, because absolute rates depend on tree size, species, and stand conditions (Wheeler et al., 2023; Chen et al., 2012)~~, as also~~ . This is seen by the large differences in absolute SF across the three selected sites (Figure 5). Instead, ~~we suggest~~ previous studies have shown that diurnal SF–VPD dynamics provide clearer insight into regulation processes ~~.~~ (Poyatos et al., 2016; Renninger et al., 2021). Therefore, the diurnal cycle of SF-VPD provides diagnostic indicators that consistently discriminate the drivers of extreme stress across all fifteen forested sites. Here we propose that two such indicators can be used in combination to identify characteristic responses to changing environmental conditions, and particularly hydrometeorological extremes. Our results show that the morning SLOPE and the AREA of the diurnal cycle of SF-VPD vary across seasons and systematically change from cold–wet to hot–dry conditions across most sites. Our results indicate that the combination of higher climatic demand and lower soil water availability reduce the coupling of SF to VPD.

We have shown~~that under~~ , that cold and wet conditions ~~, the diurnal cycles show~~ correspond to high SLOPE and low AREA ~~,~~ of the diurnal cycle (dashed lines in Figure 5, blue curves in Figure 6), as SF aligns tightly with VPD and hysteresis is minimal. This dynamics indicates a strong coupling of SF and VPD, i.e., under conditions of limited demand and high supply, trees exhibit weak stomatal regulation, prioritizing carbon uptake over preventing water losses. By contrast, in hot and dry conditions ~~,~~ (dotted lines in Figure 5, red curves in Figure 6), AREA increases and the SLOPE declines, reflecting the onset of regulation of SF before peak VPD and stagnation of SF during periods of high atmospheric demand. These patterns may result from increased stomatal regulation or limitations to plant hydraulic water supply.

Despite these general patterns, the variations of SLOPE and AREA and their relationships to hydrometeorological drivers differ among climate zones (Figures 4~~, ??~~).). AREA shows consistently positive correlations with TAir and PPFD across sites, indicating a robust response to atmospheric energy availability that is largely independent of climate regime or plant group. In

contrast, correlations between AREA and soil moisture are weaker and more variable, suggesting that AREA integrates canopy responses that are only indirectly constrained by short-term water availability.

The relationships between SLOPE and hydrometeorological drivers are markedly more site-dependent. Sites with pronounced dry seasons show positive correlations between SLOPE and soil moisture and negative correlations with TAir and PPFD, consistent with water-limited canopy dynamics. Conversely, cold and temperate sites, as well as semi-arid sites with irrigation, exhibit negative or no correlations between SLOPE and soil moisture and positive or neutral relationships with energy-related drivers, suggesting that irrigation at otherwise water-limited sites may dampen or mask typical stress-related responses. Overall, AREA behaves as a broadly comparable metric across ecosystems, primarily reflecting energy limitation, whereas SLOPE is strongly shaped by local hydrometeorological regimes and management. Together, both metrics capture differences in the strength of biosphere–atmosphere coupling.

The full exploration of the complexity of the correlations between metrics and climate drivers is beyond the scope of this analysis. Furthermore, different responses of the metrics were found across sites, but still they help to reveal whether down-regulation occurs under increasing atmospheric demand. The underlying cause of down-regulation, be it stress, adaptive behavior, or species-specific traits—must be interpreted in context. Next to site-specific differences, the still short SAPFLUXNET time series limit the calibration of the metrics against long-term means. Without such references, it remains uncertain whether regulation corresponds to stress or adaptive behavior. Importantly, a lack of regulation does not necessarily indicate optimal conditions; it may instead signal failure to respond to stress or overshooting, risking excessive water loss and hydraulic damage (Schymanski et al., 2013; Lawson et al., 2011; Jones et al., 2022; Sperry and Love, 2015).

~~Nevertheless, the~~ The metrics derived from the SF–VPD relationship ~~leave identifiable fingerprints of tree functioning under changing climates. They~~ thus can serve as early indicators of regulation patterns and water use strategies, some of which can be attributed to stress (Gambetta et al., 2020; Bodner et al., 2015; Brunner et al., 2015; Seleiman et al., 2021; Acosta-Motos et al., 2017). While SLOPE measures the strength of the coupling between SF and atmospheric demand, the AREA is an indicator of regulation timing in relationship to the atmospheric demand. Combining SLOPE and AREA helps to reduce ambiguity, as in the diagnostic case of low SLOPE with high AREA, which can be used as an indicator for strong regulation. Still, limitations remain: coarse temporal resolution may miss the identification of downregulation from breakpoint patterns in morning SF, and lack of regulation over consecutive days may reflect either risky strategies or optimal conditions. ~~Ultimately,~~ While interpreting these metrics requires integration with local water balance, species traits, and climatic drivers~~. Together, the consistent finding is that downregulation of SF in response to rising VPD reflects a fundamental trade-off: trees reduce carbon uptake to conserve water. While the meaning of this trade-off varies by site and condition, the derived metrics reliably capture its imprint in the diurnal SF–VPD hysteresis.~~ , they can serve as a useful proxy to detect changes in vegetation functioning in response to environmental conditions.

4.2 Evaluation of the state of ecosystems in focus

More detailed assessment of the hydraulic hysteresis reveals novel insights into the variation in physiological dynamics across sites, with implications for understanding their adaptation to existing climate and potential vulnerability to future climate extremes.

At the Mediterranean site (FRA_PUE), stomatal regulation is triggered when atmospheric and soil moisture drought coincide (Figure 3), reflecting interactions between water and temperature, through VPD. The sensitivity of AREA and SLOPE to both atmospheric demand and TSM is shown by the sign and strength of the correlation with all hydrometeorological drivers (Figure 4). Furthermore, the negative correlation of AREA with TSM indicates that stomatal closure is a primary response when topsoil water becomes a limiting factor. Increasing AREA ~~and the occurrence of an inverting morning breakpoint (5)~~ signals moderate regulation at high temperature, while declining SLOPE throughout the day represents strong conservative water use under severe diurnal drought and heat stress, triggering stomatal closure (Figure 4, 5, 6). A strong ability to close stomata is also indicated, when SF is absent at night at non-zero VPD. This site also has the widest range in TAir and TSM, which are as well negatively correlated, suggesting that plants frequently operate near or at their physiological limits. While the adaptation strategies have traditionally allowed these species to withstand seasonal drought, the additional compounding stress from increasing heat and VPD leaves them vulnerable to conditions that exceed historical variability (Ruffault et al., 2023; Limousin et al., 2022) . Thus, the site's long-term water conservation strategies, although beneficial in historical contexts, now signal a heightened ~~vulnerability~~ exposure to future extreme events~~, and the empirical~~ . Empirical evidence of recent mortality supports the conclusion that these adaptive strategies are being overcome under ~~novel~~ more severe and compound climatic stresses (Peguero-Pina et al., 2020; Allen et al., 2015; Aurelle et al., 2022).

In contrast, stomatal regulation at the tropical site is less sensitive to heat. Here, the SF–VPD dynamics is mostly controlled by radiation and soil moisture (Figure 4), where seasonal drought results in the decreasing of the morning SLOPE. AREA primarily reflects afternoon or nighttime stagnation of SF, which can also be a sign for high TSM enabling the trees to maintain SF during the night (Figure 5). Previous studies have shown the strong importance of VPD for SF dynamics in these regions (Horna et al., 2011; Maréchaux et al., 2018; Suárez et al., 2021), here we show that radiation still contributes to modulate the sensitivity of SF to VPD, as seen by the strong correlations between AREA and SLOPE with PPFD and ~~top soil moisture~~ TSM (Figure 4). At this site, tree height and hydraulic structure likely contribute to the high absolute SF rates, supported by deep rooting and access to water beyond topsoil layers (Horna et al., 2011; Apgaua et al., 2015; Kotowska et al., 2021; Spanner et al., 2022). The results highlight an ecosystem optimized for heat under conditions of high water supply. Trees at this site are capable of transpiring large volumes of water to maintain levels of high stomatal conductance and photosynthesis.

The Russian site displays an inverted response pattern compared to the warm sites: SLOPE and AREA increase and decrease together at the beginning of the season until they are aligned (Figure 3), which is supported by the strong correlation of AREA-PPFD and AREA-TAir (Figure 4). The cluster analysis (Figure 5) indicates that the trees at this site are predominantly energy-limited, with an optimal temperature threshold, which is likely to be occur earlier within a season with rising temperatures (Berner et al., 2013). Contrary to the other two sites, SLOPE decreases with increasing TSM, thus contradicting the expectation

that additional water would sustain SF. The variability of AREA throughout summer months might be linked to cloud cover. This suggests unusual or site-specific regulation dynamics, potentially influenced by snow melting early in the season, growth and senescence of the larch canopy, or the fact that the seasonal drought is often outside of the growing season (see Figure 3). The overall absence of strong stomatal downregulation at this site suggests that trees follow a non-conservative water-use strategy, possibly at the risk of depleting water for more carbon uptake. However, this may mask delayed stress onset or increased vulnerability to prolonged warming (Liu et al., 2022; Urban et al., 2017; Ruehr et al., 2019, 2015).

Projected climate change will likely intensify the stressors already identified here. In Mediterranean regions, increased frequency and duration of hot–dry extremes may amplify regulation and risk hydraulic failure, pointing to high vulnerability. In tropical forests, warming and drying may shift regulation triggers, potentially exposing hidden hydraulic limitations despite deep water access. At cold continental sites, continued warming may lift energy constraints, increasing SF without corresponding regulation—yet such non-conservative strategies may conceal longer-term risks of water imbalance.

4.3 Metrics and Sample Rates

Current research is actively exploring ~~the relationship between VODand various~~ how satellite-based measurements of VWC, e.g., through vegetation optical depth (VOD) or other microwave observables, and derived indicators of plant water status ~~,~~ ~~contributing~~ can contribute to a more in-depth understanding of plant health and ecosystem dynamics (Schneebeli et al. (2011), Momen et al. (2017), Holtzman et al. (2021), Humphrey and Frankenberg (2023), Asgarimehr et al. (2024)). The need for diurnal measurements of VWC to better quantify vegetation responses to drought has been highlighted by Konings et al. (2021) . As discussed in Section 1 and Figure 1, sub-daily satellite observations of vegetation water storage from microwave remote sensing can in principle be used to derive sub-daily variability in SF dynamics, a variable more directly related with plant functioning.

Here, we analysed the effect of temporal resolution on the two metrics proposed. This allows us to evaluate, in cases where 30-min or hourly resolution is not feasible, e.g., for remote-sensing applications, what the minimum temporal resolution would be required in order to adequately capture the SF–VPD dynamics. Generally, no sample rate can capture all details of the diurnal cycle as constrained by the hourly data (Figure 7).

The 8TPD represents an ideal case assuming unlimited observations or coverage, consistent with characteristic frequencies from geostationary satellites for example. While time series from measurements at 8TPD exhibit very good correlation with the reference from hourly observations of SF and VPD for AREA, the results for SLOPE already show a degradation of the signal, with a broad spread across sites. For lower sample rates, results for both metrics are less accurate than for 8TPD, with the 75% percentile for SLOPE already falling below 0.6 at 4TPD. Compared to 4TPD, the correlations of 3TPDday for SLOPE demonstrate only slight differences, since only nighttime is excluded, where sap usually does not flow significantly. Therefore, measurements at 3TPDnight, which include only nighttime flux, would not be a suitable choice for both metrics.

The mixed correlation results of SLOPE from resampled SF and VPD are likely due to the low signal-to-noise ratio of the hourly metric itself. These mixed results originate in dynamics resulting in negative SLOPE or high positive and negative outliers, such as rainy days or dew, which are hard to interpret. It is possible that SLOPE calculated from SF and VPD at

lower sample rates could better infer the signal needed for early warning of tree stress hotspots by neglecting the values of SF and VPD that produce outliers. Another potential reason for the low accuracy of SLOPE from resampled observations is the possibility of both under- and overestimation, depending on the hysteretic behavior of the diurnal cycle, which shifts the maximum value of VPD behind the maximum of SF. Furthermore, the peak times of SF and VPD at some sites (e.g. the russian site) did not match solar noon. While the dynamics at the proposed times and sample rates would be well captured at FRA_PUE and GUF_GUY_GUY, both metrics of the diurnal cycle could be underestimated at sites with dynamics similar to RUS_POG_VAR.

These results raise the question of whether the choice of metrics is adequate to capture the diurnal cycle of SF and VPD from satellites and how they can be improved. AREA is generally underestimated, but relative trends in AREA tend to be consistently retrieved with coarser temporal resolution. ~~Even if resampled~~ SLOPE has lower ~~coefficients of determination~~ Pearson R^2 than AREA, ~~it indicates~~ however, the relative trends are still sufficient to indicate water limitation at most sites. Nevertheless, alternative approaches should be evaluated. For example, instead of the absolute slope, the ratio of the actual to a potential morning regression slope could be considered. This metric could identify collapse days, when the ratio is high, and exclude outliers when it exceeds 1. The challenge here mainly lies in how a potential slope could be defined.

~~Furthermore, the relationship between sub-daily VOD and SF velocity data needs to be evaluated to determine the optimal final sample rates.~~ The reduced variance of the metrics under high environmental stress conditions indicates a stabilization of underlying processes and enhances the predictability of stress patterns during these periods. Therefore, SLOPE and AREA can detect early warning signs of SF regulation, which indicates tree health, from the sub-daily response of SF to VPD, which could then be further investigated in detail through in situ observations to enhance our knowledge of specific stress responses outside of laboratory settings and mitigate subsequent tree mortality events. For this purpose, a sample rate of 3TPD centered at day-time, would suffice.

4.4 Linking fluxes to storage

One limitation of the current study is the reliance on sap flow data (a flux), while the the quantity more likely to be provided by satellite remote sensing is VOD (or derived VWC), a measure of vegetation water storage.

Recall from Figure 1 that the expected shapes of the hysteresis curves are different for SF and VWC. It is therefore possible that a SLOPE metric may be more reliably estimated when monitoring VWC rather than SF under a 3TPDday scenario. The application of conservation of mass to translate between the two is complicated by a mismatch in terms of the volume being considered. Sap flow measurements quantify the movement of water through the sapwood of individual tress. Although sensing depth of VOD and its sensitivity to water content in different compartments of the vegetation are known to depend on frequency, VOD (and derived VWC or biomass) are commonly assumed to represent storage of the vegetation as a whole, and spatially integrated across some footprint. Therefore, the dynamics observed in sap flow data, and the derived daily slope and area metrics should not be considered a trivial proxy for VOD or a change in VOD. That said, sap flow data reveal when transpiration is occurring which allows us to identify when, and the degree to which storage is likely to be changing at sub-daily scales. While it seems logical that steeper slopes and larger areas in sap flow would also result in similar changes in VOD, this

should be confirmed with sub-daily VOD estimates from tower-based radars and/or radiometers and emerging GNSS-related techniques ~~.~~ (Jagdhuber et al., 2025).

5 Conclusions

The aim of this study was to understand how sub-daily sap flow dynamics can be used as an indicator of vegetation functioning and stress and to evaluate the potential to estimate descriptors of the diurnal cycle using temporally sparse data. While sap flow alone has limited interpretability in assessing vegetation condition, its response to sub-daily atmospheric water demand variations can help identify different types of stress. We propose two ~~metrics~~ simple descriptors of the diurnal cycle of SF–VPD, namely the morning sensitivity of SF to VPD (the slope) and the area of the hysteresis curve, ~~the SLOPE, describing the SF sensitivity to VPD during the morning and the AREA describing the magnitude of diurnal hysteresis ,~~ that show clear seasonal and interannual variability patterns, associated with varying ~~temperature and water availability~~ hydrometeorological conditions. As interpretion of either metric alone can be ambiguous, it is recommended that these metrics should be interpreted in combination.

Our results show that the descriptors of short-term dynamics in SF response to atmospheric water demand ~~can reflect long-term responses to stressors,~~ reflect responses to hydroclimatic stressors, and are particularly sensitive to extreme events, emphasizing the potential for observations of sub-daily vegetation water dynamics to monitor ecosystem vitality at larger scales. Given the lack of global measurements of SF or vegetation water content at high temporal resolution from which to derive such metrics, we ~~analyse their dependence on temporal sampling . Decreasing the sampling rate to 6-hourly at 4~~ show that a sampling rate of 3–4 times per day ~~or even 3 times per day is~~ would be sufficient to derive ~~these two metrics and retain some of~~ the two descriptors proposed while retaining the information of the finer temporal resolution ~~measurement. However the morning SLOPE requires finer sampling than the AREA, which indicates hysteresis strength. Nevertheless, our results~~ measurements. Our results thus show potential for temporally and spatially continuous measurements, e.g., from future satellite missions, to use sub-daily information about vegetation water content and fluxes to track plant stress as an early-warning indicator for mortality events.

Therefore, enhanced vegetation monitoring through ~~high-resolution~~ sub-daily satellite observations of vegetation water content could greatly improve ecosystem management strategies and climate change mitigation plans.

Code availability. The code can be made publicly available upon publication.

Data availability. The data is publicly available in the SAPFLUXNET database (Poyatos et al., 2019) (last access: 27 October 2025).

Appendix A

A1

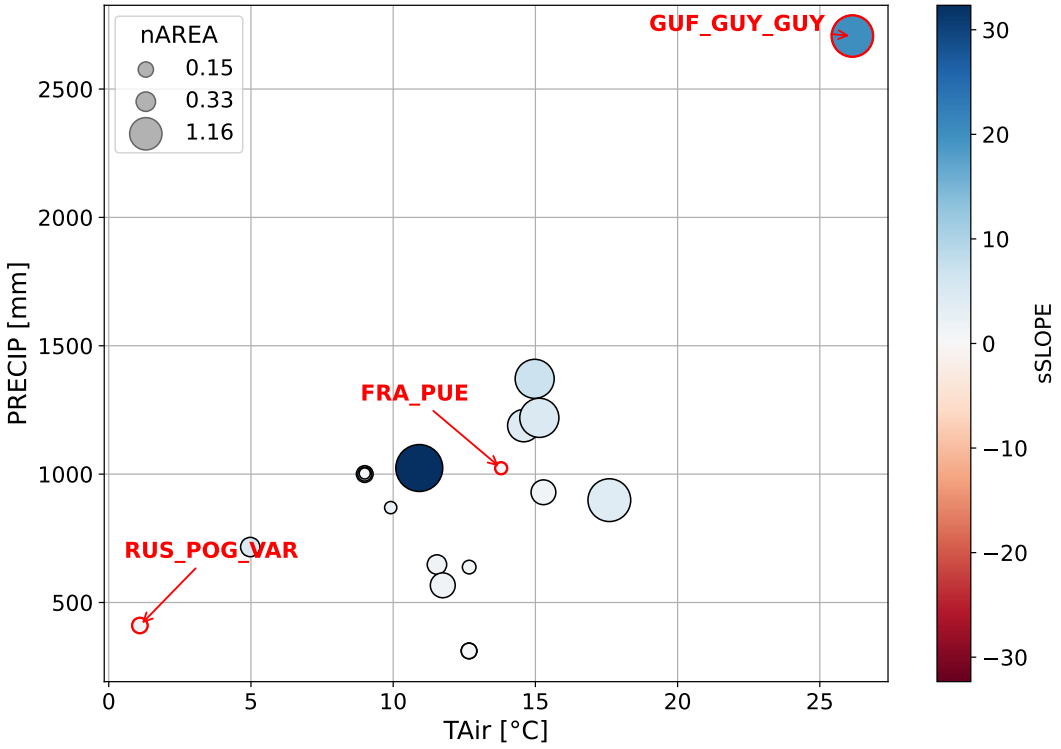

Figure A1. Mean precipitation and mean air temperature at each of the ~~33~~ study sites. Symbol size scales with median sAREA and color indicates median sSLOPE per site across years with the three selected sites annotated and highlighted in red.

~~Maps of Pearson's correlation coefficients between the seasonal cycles of SLOPE and AREA and those of the hydrometeorological drivers (TSM, TAir, PPFD) at each site. These correlations illustrate the climatic factors associated with the seasonal evolution of the metrics.~~

Table A1: Site characteristics including physical and biological attributes.

Site	DBH_mean (cm)	LAI	Soil texture	Species	Biome	Plant group
AUS_RIC_EUC_ELE	36.59	2.0	sandy loam	Eucalyptus tereticornis	Woodland/Shrubland	angiosperm

Continued on next page

Table A1 – *Continued from previous page*

Site	DBH_mean (cm)	LAI	Soil texture	Species	Biome	Plant group
AUS_WOM	37.50	2.2	loam	Eucalyptus rubida, Eucalyptus obliqua	Temperate forest	angiosperm
CAN_TUR_P39_POS	40.41	5.3	sand	Pinus strobus	Temperate forest	gymnosperm
CAN_TUR_P39_PRE	39.98	5.3	sand	Pinus strobus	Temperate forest	gymnosperm
CAN_TUR_P74	19.13	6.7	sand	Pinus strobus	Temperate forest	gymnosperm
CHE_LOT_NOR	34.68	—	loam	Larix decidua, Picea abies	Temperate forest	gymnosperm
ESP_ALT_ARM	21.14	1.1	clay	Pinus nigra, Quercus ilex, Quercus faginea	Woodland/Shrubland	mixed
ESP_ALT_TRI	24.18	—	—	Pinus nigra, Quercus ilex	Woodland/Shrubland	mixed
FRA_PUE	9.12	2.4	clay loam	Quercus ilex	Woodland/Shrubland	angiosperm
GUF_GUY_GUY	37.62	7.0	sandy clay	Sloanea sp, Vacapoua americana, Licania membranacea, Oxandra asbeckii, Iryanthera sagotiana, Goupia glabra	Tropical rain forest	angiosperm
NLD_LOO	27.15	2.2	sand	Pinus sylvestris	Woodland/Shrubland	gymnosperm
NZL_HUA_HUA	81.67	—	—	Agathis australis	Temperate forest	gymnosperm
RUS_POG_VAR	21.83	—	—	Larix sibirica Ledeb., Larix gmelinii, Pinus sibirica	Woodland/Shrubland	gymnosperm

Continued on next page

Table A1 – *Continued from previous page*

Site	DBH_mean (cm)	LAI	Soil texture	Species	Biome	Plant group
USA_DUK_HAR	37.66	7.0	loam	Liriodendron tulipifera, Liquidambar styraciflua, Carya tomentosa, Quercus alba, Quercus michauxii, Quercus phellos	Temperate forest	angiosperm
USA_HIL_HF1_POS	17.22	2.6	clay loam	Pinus taeda, Liquidambar styraciflua, Acer rubrum, Quercus spp., Liriodendron tulipifera	Temperate forest	mixed
USA_HIL_HF2	25.30	5.5	loam	Pinus taeda, Liriodendron tulipifera, Acer rubrum, Liquidambar styraciflua, Fagus grandifolia, Quercus spp., Pinus virginiana	Temperate forest	mixed
USA_PJS_P04_AMB	25.92	0.7	sandy loam	Pinus edulis, Juniperus monosperma	Temperate grassland desert	gymnosperm
USA_PJS_P08_AMB	32.83	0.9	sandy loam	Pinus edulis, Juniperus monosperma	Temperate grassland desert	gymnosperm
USA_PJS_P12_AMB	30.60	0.7	sandy loam	Pinus edulis, Juniperus monosperma	Temperate grassland desert	gymnosperm
ZAF_NOO_E3_IRR	9.92	3.4	sand	Malus domestica	Woodland/Shrubland	angiosperm
ZAF_SOU_SOU	45.55	3.0	loam	Malus domestica	Woodland/Shrubland	angiosperm

Table A2: Site treatments and references.

Site	Management	Reference
AUS_RIC_EUC_ELE	Naturally regenerated, unmanaged	https://doi.org/10.1111/1365-2435.12532
AUS_WOM	Naturally regenerated, unmanaged	http://dx.doi.org/10.1016/j.foreco.2016.12.017
CAN_TUR_P39_POS	Plantation, managed	https://doi.org/10.1016/j.agrformet.2010.04.008
CAN_TUR_P39_PRE	Plantation, managed	https://doi.org/10.1016/j.agrformet.2010.04.008
CAN_TUR_P74	Plantation, managed	https://doi.org/10.1016/j.agrformet.2010.04.008
CHE_LOT_NOR	Naturally regenerated, unmanaged	https://doi.org/10.1111/pce.13500
ESP_ALT_ARM	Naturally regenerated, unmanaged	https://doi.org/10.1007/s11258-014-0351-x
ESP_ALT_TRI	Naturally regenerated, unmanaged	https://doi.org/10.1007/s10342-013-0687-0
FRA_PUE	Naturally regenerated, unmanaged	https://doi.org/10.1111/j.1365-2486.2009.01852.x
GUF_GUY_GUY	Naturally regenerated, unmanaged	https://doi.org/10.1111/j.1365-2486.2008.01610.x
NLD_LOO	Plantation, unmanaged	https://doi.org/10.1016/j.agrformet.2011.07.020
NZL_HUA_HUA	Naturally regenerated, unmanaged	https://doi.org/10.1007/s00468-015-1164-9
RUS_POG_VAR	Plantation, managed	https://doi.org/10.1016/j.agrformet.2019.02.038
USA_DUK_HAR	Naturally regenerated, unmanaged	http://dx.doi.org/10.1016/j.agrformet.2008.06.013
USA_HIL_HF1_POS	Naturally regenerated, unmanaged	https://doi.org/10.1002/hyp.10474
USA_HIL_HF2	Naturally regenerated, unmanaged	https://doi.org/10.1002/hyp.10474
USA_PJS_P04_AMB	Naturally regenerated, unmanaged	http://dx.doi.org/10.1890/ES11-00369.1
USA_PJS_P08_AMB	Naturally regenerated, unmanaged	http://dx.doi.org/10.1890/ES11-00369.1
USA_PJS_P12_AMB	Naturally regenerated, unmanaged	http://dx.doi.org/10.1890/ES11-00369.1
ZAF_NOO_E3_IRR	Orchard	https://doi.org/10.1016/j.agrformet.2019.02.042
ZAF_SOU_SOU	Orchard	https://doi.org/10.1016/j.agwat.2018.06.017

Author contributions. AB, SSD, and AS designed the study. AS conducted the analysis with scientific input from AB, SSD, and DM. AS wrote the first draft of the paper and prepared all figures, including the conceptual representation. JML contributed site expertise and additional data from the FRA_PUE site, which shaped the idea. All authors contributed to manuscript revision and approved the submitted version.

Competing interests. The authors declare that they have no conflict of interest.

Acknowledgements. The work was supported by the European Space Agency (SLAINTE, 4000139242/22/NL/SD).

References

Contrasting diel hysteresis between soil autotrophic and heterotrophic respiration in a desert ecosystem under different rainfall scenarios. 5. ISSN 2045-2322. https://doi.org/10.1038/srep16779. URL https://www.nature.com/articles/srep16779.

Jose Ramón Acosta-Motos, Maria Fernanda Ortuño, Agustina Bernal-Vicente, Pedro Diaz-Vivancos, Maria Jesus Sanchez-Blanco, and Jose Antonio Hernandez. Plant responses to salt stress: Adaptive mechanisms. *Agronomy*, 7(1):18, 2017. https://doi.org/10.3390/agronomy7010018. URL https://doi.org/10.3390/agronomy7010018. Special Issue: Further Metabolism in Plant System.

Maricar Aguilos, Bruno Hérault, Benoit Burban, Fabien Wagner, and Damien Bonal. What drives long-term variations in carbon flux and balance in a tropical rainforest in French Guiana? *Agricultural and Forest Meteorology*, 253-254:114–123, May 2018. ISSN 0168-1923. https://doi.org/10.1016/j.agrformet.2018.02.009. URL https://www.sciencedirect.com/science/article/pii/S0168192318300595.

V. ALLARD, J. M. OURCIVAL, S. RAMBAL, R. JOFFRE, and A. ROCHETEAU. Seasonal and annual variation of carbon exchange in an evergreen mediterranean forest in southern france. *Global Change Biology*, 14(4):714–725, 2008. https://doi.org/https://doi.org/10.1111/j.1365-2486.2008.01539.x. URL https://onlinelibrary.wiley.com/doi/abs/10.1111/j.1365-2486.2008.01539.x.

Craig D. Allen, David D. Breshears, and Nate G. McDowell. On underestimation of global vulnerability to tree mortality and forest die-off from hotter drought in the Anthropocene. *Ecosphere*, 6(8):art129, 2015. ISSN 2150-8925. https://doi.org/10.1890/ES15-00203.1. URL https://onlinelibrary.wiley.com/doi/abs/10.1890/ES15-00203.1. _eprint: https://onlinelibrary.wiley.com/doi/pdf/10.1890/ES15-00203.1.

Deborah M. G. Apgaua, Françoise Y. Ishida, David Y. P. Tng, Melinda J. Laidlaw, Rubens M. Santos, Rizwana Rumman, Derek Eamus, Joseph A. M. Holtum, and Susan G. W. Laurance. Functional traits and water transport strategies in lowland tropical rainforest trees. *PLOS ONE*, 10(6):e0130799, 2015. https://doi.org/10.1371/journal.pone.0130799. URL https://doi.org/10.1371/journal.pone.0130799.

Milad Asgarimehr, Dara Entekhabi, and Adriano Camps. Diurnal Vegetation Moisture Cycle in the Amazon and Response to Water Stress. *Geophysical Research Letters*, 51(19):e2024GL111462, October 2024. ISSN 0094-8276, 1944-8007. https://doi.org/10.1029/2024GL111462. URL https://agupubs.onlinelibrary.wiley.com/doi/10.1029/2024GL111462.

Didier Aurelle, Séverine Thomas, Cécile Albert, Marc Bally, Alberte Bondeau, Charles-François Boudouresque, Abigail E. Cahill, François Carlotti, Anne Chenuil, Wolfgang Cramer, Hendrik Davi, Aurélien De Jode, Alexander Ereskovsky, Anne-Marie Farnet, Catherine Fernandez, Thierry Gauquelin, Pascal Mirleau, Anne-Christine Monnet, Bernard Prévosto, Vincent Rossi, Stéphane Sartoretto, France Van Wambeke, and Bruno Fady. Biodiversity, climate change, and adaptation in the mediterranean. *Ecosphere*, 13(4):e3915, 2022. https://doi.org/https://doi.org/10.1002/ecs2.3915. URL https://esajournals.onlinelibrary.wiley.com/doi/abs/10.1002/ecs2.3915.

A. P. Barchenkov, I. A. Petrov, A. S. Shushpanov, and A. S. Golyukov. Climatic Response of Larch (Larix sp.) Radial Increment in Provenances on the Krasnoyarsk Forest Steppe. *Contemporary Problems of Ecology*, 16(5):620–630, October 2023. ISSN 1995-4263. https://doi.org/10.1134/S1995425523050025. URL https://doi.org/10.1134/S1995425523050025.

Ana Bastos, René Orth, Markus Reichstein, Philippe Ciais, Nicolas Viovy, Sönke Zaehle, Peter Anthoni, Almut Arneth, Pierre Gentine, Emilie Joetzjer, Sebastian Lienert, Tammas Loughran, Patrick C. McGuire, Sungmin O, Julia Pongratz, and Stephen Sitch. Vulnerability of European ecosystems to two compound dry and hot summers in 2018 and 2019. *Earth System Dynamics*, 12(4):1015–1035, October 2021. ISSN 2190-4979. https://doi.org/10.5194/esd-12-1015-2021. URL https://esd.copernicus.org/articles/12/1015/2021/.

Paulo N Bernardino, Rafael S Oliveira, Koenraad Van Meerbeek, Marina Hirota, Mariana N Furtado, Isabela A Sanches, and Ben Somers. Estimating vegetation water content from sentinel-1 c-band sar data over savanna and grassland ecosystems. *Environmental Research Letters*, 19(3):034019, feb 2024. https://doi.org/10.1088/1748-9326/ad288f. URL https://doi.org/10.1088/1748-9326/ad288f.

Logan T. Berner, Pieter S. A. Beck, Andrew G. Bunn, and Scott J. Goetz. Plant response to climate change along the forest-tundra ecotone in northeastern siberia. *Global Change Biology*, 19(11):3449–3462, 2013. https://doi.org/10.1111/gcb.12304. URL https://doi.org/10.1111/gcb.12304.

Gernot Bodner, Alireza Nakhforoosh, and Hans-Peter Kaul. Management of crop water under drought: A review. *Agronomy for Sustainable Development*, 35(2):401–442, 2015. ISSN 1773-0155. https://doi.org/10.1007/s13593-015-0283-4. URL https://doi.org/10.1007/s13593-015-0283-4.

Damien Bonal, Alexandre Bosc, Stéphane Ponton, Jean-Yves Goret, Benoît Burban, Patrick Gross, Jean-Marc Bonnefond, Jan Elbers, Bernard Longdoz, Daniel Epron, Jean-Marc Guehl, and André Granier. Impact of severe dry season on net ecosystem exchange in the Neotropical rainforest of French Guiana. *Global Change Biology*, 14(8):1917–1933, 2008. ISSN 1365-2486. https://doi.org/10.1111/j.1365-2486.2008.01610.x. URL https://onlinelibrary.wiley.com/doi/abs/10.1111/j.1365-2486.2008.01610.x. _eprint: https://onlinelibrary.wiley.com/doi/pdf/10.1111/j.1365-2486.2008.01610.x.

Ivano Brunner, Claude Herzog, Melissa A. Dawes, Matthias Arend, and Christoph Sperisen. How tree roots respond to drought. *Frontiers in Plant Science*, 6:547, 2015. https://doi.org/10.3389/fpls.2015.00547. URL https://doi.org/10.3389/fpls.2015.00547.

Mercedes Bustamante, Joyashree Roy, Daniel Ospina, Ploy Achakulwisut, Anubha Aggarwal, Ana Bastos, Wendy Broadgate, Josep G. Canadell, Edward R. Carr, Deliang Chen, Helen A. Cleugh, Kristie L. Ebi, Clea Edwards, Carol Farbotko, Marcos Fernández-Martínez, Thomas L. Frölicher, Sabine Fuss, Oliver Geden, Nicolas Gruber, Luke J. Harrington, Judith Hauck, Zeke Hausfather, Sophie Hebden, Aniek Hebinck, Saleemul Huq, Matthias Huss, M. Laurice P. Jamero, Sirkku Juhola, Nilushi Kumarasinghe, Shuaib Lwasa, Bishawjit Mallick, Maria Martin, Steven McGreevy, Paula Mirazo, Aditi Mukherji, Greg Muttitt, Gregory F. Nemet, David Obura, Chukwumerije Okereke, Tom Oliver, Ben Orlove, Nadia S. Ouedraogo, Prabir K. Patra, Mark Pelling, Laura M. Pereira, Åsa Persson, Julia Pongratz, Anjal Prakash, Anja Rammig, Colin Raymond, Aaron Redman, Cristobal Reveco, Johan Rockström, Regina Rodrigues, David R. Rounce, E. Lisa F. Schipper, Peter Schlosser, Odirilwe Selomane, Gregor Semieniuk, Yunne-Jai Shin, Tasneem A. Siddiqui, Vartika Singh, Giles B. Sioen, Youba Sokona, Detlef Stammer, Norman J. Steinert, Sunhee Suk, Rowan Sutton, Lisa Thalheimer, Vikki Thompson, Gregory Trencher, Kees van der Geest, Saskia E. Werners, Thea Wübbelmann, Nico Wunderling, Jiabo Yin, Kirsten Zickfeld, and Jakob Zscheischler. Ten new insights in climate science 2023. *Global Sustainability*, 7:e19, January 2023. ISSN 2059-4798. https://doi.org/10.1017/sus.2023.25. URL https://www.cambridge.org/core/journals/global-sustainability/article/ten-new-insights-in-climate-science-2023/F7F1C10C07FD241BFE30ACC4BA555A56.

A. Chakir, P.L. Frison, S. Khabba, J. Ezzahar, L. Villard, P. Fanise, N. Ouaadi, V. Ledantec, and L. Jarlan. Diurnal Cycles of C-Band Temporal Coherence and Backscattering Coefficient Over an Olive Orchard in a Semi-Arid Area: Comparison of In Situ and Sentinel-1 Radar Observations. In *2021 IEEE International Geoscience and Remote Sensing Symposium IGARSS*, pages 3801–3804, July 2021. https://doi.org/10.1109/IGARSS47720.2021.9553129.

Lixin Chen, Zhiqiang Zhang, and Brent E. Ewers. Urban tree species show the same hydraulic response to vapor pressure deficit across varying tree size and environmental conditions. *PLOS ONE*, 7(10):e47882, 2012. https://doi.org/10.1371/journal.pone.0047882. URL https://doi.org/10.1371/journal.pone.0047882.

Brendan Choat, Timothy J. Brodribb, Craig R. Brodersen, Remko A. Duursma, Rosana López, and Belinda E. Medlyn. Triggers of tree mortality under drought. 558(7711):531–539. ISSN 1476-4687. https://doi.org/10.1038/s41586-018-0240-x. URL https://www.nature.com/articles/s41586-018-0240-x. Publisher: Nature Publishing Group.

B. J. Choudhury and C. J. Tucker. Monitoring global vegetation using nimbus-7 37 ghz data – some empirical relations. *International Journal of Remote Sensing*, 8(7):1085–1090, 1987. ISSN 0143-1161.

V. Cicuéndez, J. Litago, M. Huesca, et al. Assessment of the gross primary production dynamics of a mediterranean holm oak forest by remote sensing time series analysis. *Agroforestry Systems*, 89(3):491–510, 2015. https://doi.org/10.1007/s10457-015-9786-x. URL https://doi.org/10.1007/s10457-015-9786-x.

Jon Cranko Page, Martin G. De Kauwe, Gab Abramowitz, Jamie Cleverly, Nina Hinko-Najera, Mark J. Hovenden, Yao Liu, Andy J. Pitman, and Kiona Ogle. Examining the role of environmental memory in the predictability of carbon and water fluxes across Australian ecosystems. *Biogeosciences*, 19(7):1913–1932, April 2022. ISSN 1726-4170. https://doi.org/10.5194/bg-19-1913-2022. URL https://bg.copernicus.org/articles/19/1913/2022/.

S. D. Davis and H. A. Mooney. Water use patterns of four co-occurring chaparral shrubs. 70(2):172–177. ISSN 1432-1939. https://doi.org/10.1007/BF00379236. URL https://doi.org/10.1007/BF00379236.

Tim Van Emmerik, Susan Steele-Dunne, Rolf Hut, Pierre Gentine, Marceau Guerin, Rafael S. Oliveira, Jim Wagner, John Selker, and Nick Van de Giesen. Measuring tree properties and responses using low-cost accelerometers. *Sensors*, 17(5):1098, 2017. https://doi.org/10.3390/s17051098. URL https://doi.org/10.3390/s17051098.

Michael A. Forster. How significant is nocturnal sap flow? *Tree Physiology*, 34(7):757–765, July 2014. ISSN 0829-318X. https://doi.org/10.1093/treephys/tpu051. URL https://doi.org/10.1093/treephys/tpu051.

Peter J. Franks, Joseph A. Berry, Danica L. Lombardozzi, and Gordon B. Bonan. Stomatal Function across Temporal and Spatial Scales: Deep-Time Trends, Land-Atmosphere Coupling and Global Models. *Plant Physiology*, 174(2):583–602, June 2017. ISSN 0032-0889. https://doi.org/10.1104/pp.17.00287. URL https://doi.org/10.1104/pp.17.00287.

Frédéric Frappart, Jean-Pierre Wigneron, Xiaojun Li, Xiangzhuo Liu, Amen Al-Yaari, Lei Fan, Mengjia Wang, Christophe Moisy, Erwan Le Masson, Zacharie Aoulad Lafkih, Clément Vallé, Bertrand Ygorra, and Nicolas Baghdadi. Global Monitoring of the Vegetation Dynamics from the Vegetation Optical Depth (VOD): A Review. *Remote Sensing*, 12(18):2915, January 2020. ISSN 2072-4292. https://doi.org/10.3390/rs12182915. URL https://www.mdpi.com/2072-4292/12/18/2915. Number: 18 Publisher: Multidisciplinary Digital Publishing Institute.

J. C. Friesen. Regional vegetation water effects on satellite soil moisture estimations for West Africa. *Ecology and Development Series 63*, 2008. URL https://repository.tudelft.nl/islandora/object/uuid%3A81ef59db-f20d-4bc7-a539-e6f08f2cbd0a.

Steve Frolking, Tom Milliman, Michael Palace, Dominik Wisser, Richard Lammers, and Mark Fahnestock. Tropical forest backscatter anomaly evident in SeaWinds scatterometer morning overpass data during 2005 drought in Amazonia. *Remote Sensing of Environment*, 115(3):897–907, March 2011. ISSN 0034-4257. https://doi.org/10.1016/j.rse.2010.11.017. URL https://www.sciencedirect.com/science/article/pii/S0034425710003366.

Gregory A. Gambetta, Jose Carlos Herrera, Silvina Dayer, Quishuo Feng, Uri Hochberg, and Simone D. Castellarin. The physiology of drought stress in grapevine: Towards an integrative definition of drought tolerance. *Journal of Experimental Botany*, 71(16):4658–4676, 2020. ISSN 0022-0957. https://doi.org/10.1093/jxb/eraa245. URL https://doi.org/10.1093/jxb/eraa245.

A. Hamadi, C. Albinet, P. Borderies, T. Koleck, L. Villard, D. Ho Tong Minh, and T. Le Toan. Temporal Survey of Polarimetric P-Band Scattering of Tropical Forests. *IEEE Transactions on Geoscience and Remote Sensing*, 52(8):4539–4547, August 2014. ISSN 1558-0644. https://doi.org/10.1109/TGRS.2013.2282357.

William M. Hammond, Daniel M. Johnson, and Frederick C. Meinzer. A thin line between life and death: Radial sap flux failure signals trajectory to tree mortality. *Plant, Cell & Environment*, 44(5):1311–1314, May 2021. ISSN 0140-7791. https://doi.org/10.1111/pce.14033. URL https://onlinelibrary.wiley.com/doi/full/10.1111/pce.14033. Publisher: John Wiley & Sons, Ltd.

Henrik Hartmann, Ana Bastos, Adrian J Das, Adriane Esquivel-Muelbert, William M Hammond, Jordi Martínez-Vilalta, Nate G McDowell, Jennifer S Powers, Thomas AM Pugh, and Katinka X Ruthrof. Climate change risks to global forest health: emergence of unexpected events of elevated tree mortality worldwide. *Annual Review of Plant Biology*, 73:673–702, 2022. ISSN 1543-5008.

D. Ho Tong Minh, S. Tebaldini, F. Rocca, T. Le Toan, P. Borderies, T. Koleck, C. Albinet, L. Villard, and A. Hamadi. Temporal decorrelation in tropical forest: results from TropiScat and implications for BIOMASS tomography. In *2013 IEEE International Geoscience and Remote Sensing Symposium - IGARSS*, pages 1206–1209, July 2013. https://doi.org/10.1109/IGARSS.2013.6722996.

Nataniel Holtzman, Leander D. L. Anderegg, Simon Kraatz, Alex Mavrovic, Oliver Sonnentag, Christoforos Pappas, Michael H. Cosh, Alexandre Langlois, Tarendra Lakhankar, Derek Tesser, Nicholas Steiner, Andreas Colliander, Alexandre Roy, and Alexandra G. Konings. L-band vegetation optical depth as an indicator of plant water potential in a temperate deciduous forest stand. *Biogeosciences*, 18(2):739–753, February 2021. ISSN 1726-4170. https://doi.org/10.5194/bg-18-739-2021. URL https://bg.copernicus.org/articles/18/739/2021/. Publisher: Copernicus GmbH.

Nataniel Holtzman, Yujie Wang, Jeffrey D. Wood, Christian Frankenberg, and Alexandra G. Konings. Constraining Plant Hydraulics With Microwave Radiometry in a Land Surface Model: Impacts of Temporal Resolution. *Water Resources Research*, 59(11):e2023WR035481, 2023. ISSN 1944-7973. https://doi.org/10.1029/2023WR035481. URL https://onlinelibrary.wiley.com/doi/abs/10.1029/2023WR035481. _eprint: https://onlinelibrary.wiley.com/doi/pdf/10.1029/2023WR035481.

Viviana Horna, Bernhard Schuldt, Sarah Brix, and Christoph Leuschner. Environment and tree size controlling stem sap flux in a perhumid tropical forest of central sulawesi, indonesia. *Annals of Forest Science*, 68(5):1027–1038, 2011. ISSN 1297-966X. https://doi.org/10.1007/s13595-011-0110-2. URL https://doi.org/10.1007/s13595-011-0110-2.

Vincent Humphrey and Christian Frankenberg. Continuous ground monitoring of vegetation optical depth and water content with GPS signals. *Biogeosciences*, 20(9):1789–1811, May 2023. ISSN 1726-4170. https://doi.org/10.5194/bg-20-1789-2023. URL https://bg.copernicus.org/articles/20/1789/2023/. Publisher: Copernicus GmbH.

Thomas Jagdhuber, Anne-Sophie Schmidt, Anke Fluhrer, David Chaparro, François Jonard, María Piles, Natan Holtzman, Alexandra G. Konings, Alexander Feldman, Michael J. Baur, Susan Steele-Dunne, Karin Schellenberg, and Harald Kunstmann. Estimation of forest water potential from ground-based l-band radiometry. *IEEE Journal of Selected Topics in Applied Earth Observations and Remote Sensing*, 2025. https://doi.org/10.1109/JSTARS.2025.3533567.

P. G. Jarvis and K. G. McNaughton. Stomatal Control of Transpiration: Scaling Up from Leaf to Region. In A. MacFadyen and E. D. Ford, editors, *Advances in Ecological Research*, volume 15, pages 1–49. Academic Press, January 1986a. https://doi.org/10.1016/S0065-2504(08)60119-1. URL https://www.sciencedirect.com/science/article/pii/S0065250408601191.

P.G. Jarvis and K.G. McNaughton. Stomatal control of transpiration: Scaling up from leaf to region. *Advances in Ecological Research*, 15:1–49, 1986b. ISSN 0065-2504. https://doi.org/https://doi.org/10.1016/S0065-2504(08)60119-1. URL https://www.sciencedirect.com/science/article/pii/S0065250408601191.

Simon Jones, Cleiton B. Eller, and Peter M. Cox. Application of feedback control to stomatal optimisation in a global land surface model. *Frontiers in Environmental Science*, 10:970266, 2022. https://doi.org/10.3389/fenvs.2022.970266. URL https://doi.org/10.3389/fenvs.2022.970266.

S. Khabbazan, S. C. Steele-Dunne, P. Vermunt, J. Judge, M. Vreugdenhil, and G. Gao. The influence of surface canopy water on the relationship between L-band backscatter and biophysical variables in agricultural monitoring. *Remote Sensing of Environment*, 268: 112789, January 2022. ISSN 0034-4257. https://doi.org/10.1016/j.rse.2021.112789. URL https://www.sciencedirect.com/science/article/pii/S0034425721005095.

Alexandra G. Konings, Maria Piles, Narendra Das, and Dara Entekhabi. L-band vegetation optical depth and effective scattering albedo estimation from smap. *Remote Sensing of Environment*, 198:460–470, 2017. ISSN 0034-4257. https://doi.org/https://doi.org/10.1016/j.rse.2017.06.037. URL https://www.sciencedirect.com/science/article/pii/S0034425717302961.

Alexandra G. Konings, Krishna Rao, and Susan C. Steele-Dunne. Macro to micro: microwave remote sensing of plant water content for physiology and ecology. *New Phytologist*, 223(3):1166–1172, 2019. ISSN 1469-8137. https://doi.org/10.1111/nph.15808. URL https://onlinelibrary.wiley.com/doi/abs/10.1111/nph.15808. _eprint: https://onlinelibrary.wiley.com/doi/pdf/10.1111/nph.15808.

Alexandra G. Konings, Sassan S. Saatchi, Christian Frankenberg, Michael Keller, Victor Leshyk, William R. L. Anderegg, Vincent Humphrey, Ashley M. Matheny, Anna Trugman, Lawren Sack, Elizabeth Agee, Mallory L. Barnes, Oliver Binks, Kerry Cawse-Nicholson, Bradley O. Christoffersen, Dara Entekhabi, Pierre Gentine, Nataniel M. Holtzman, Gabriel G. Katul, Yanlan Liu, Marcos Longo, Jordi Martinez-Vilalta, Nate McDowell, Patrick Meir, Maurizio Mencuccini, Assaad Mrad, Kimberly A. Novick, Rafael S. Oliveira, Paul Siqueira, Susan C. Steele-Dunne, David R. Thompson, Yujie Wang, Richard Wehr, Jeffrey D. Wood, Xiangtao Xu, and Pieter A. Zuidema. Detecting forest response to droughts with global observations of vegetation water content. *Global Change Biology*, 27(23):6005–6024, 2021. ISSN 1365-2486. https://doi.org/10.1111/gcb.15872. URL https://onlinelibrary.wiley.com/doi/abs/10.1111/gcb.15872. _eprint: https://onlinelibrary.wiley.com/doi/pdf/10.1111/gcb.15872.

Martyna M. Kotowska, Roman M. Link, Alexander Röll, Dietrich Hertel, Dirk Hölscher, Pierre-André Waite, Gerald Moser, Aiyen Tjoa, Christoph Leuschner, and Bernhard Schuldt. Effects of wood hydraulic properties on water use and productivity of tropical rainforest trees. *Frontiers in Forests and Global Change*, 3:598759, 2021. ISSN 2624-893X. https://doi.org/10.3389/ffgc.2020.598759. URL https://www.frontiersin.org/journals/forests-and-global-change/articles/10.3389/ffgc.2020.598759.

Joe Landsberg, Richard Waring, and Michael Ryan. Water relations in tree physiology: where to from here? *Tree Physiology*, 37(1):18–32, January 2017. ISSN 0829-318X. https://doi.org/10.1093/treephys/tpw102. URL https://doi.org/10.1093/treephys/tpw102.

Tracy Lawson, Susanne von Caemmerer, and Irene Baroli. *Photosynthesis and Stomatal Behaviour*, pages 265–304. Springer Berlin Heidelberg, Berlin, Heidelberg, 2011. ISBN 978-3-642-13145-5. https://doi.org/10.1007/978-3-642-13145-5_11. URL https://doi.org/10.1007/978-3-642-13145-5_11.

Jean-Marc Limousin, S. Rambal, J. M. Ourcival, A. Rocheteau, R. Joffre, and R. Rodriguez-Cortina. Long-term transpiration change with rainfall decline in a mediterranean quercus ilex forest. 15(9):2163–2175, 2009. ISSN 1365-2486. https://doi.org/10.1111/j.1365-2486.2009.01852.x. URL https://onlinelibrary.wiley.com/doi/abs/10.1111/j.1365-2486.2009.01852.x. _eprint: https://onlinelibrary.wiley.com/doi/pdf/10.1111/j.1365-2486.2009.01852.x.

Jean-Marc Limousin, Damien Longepierre, Roland Huc, and Serge Rambal. Change in hydraulic traits of mediterranean quercus ilex subjected to long-term throughfall exclusion. *Tree Physiology*, 30(8):1026–1036, 07 2010a.

Jean-Marc Limousin, Laurent Misson, Anne-Violette Lavoir, Nicolas K. Martin, and Serge Rambal. Do photosynthetic limitations of evergreen Quercus ilex leaves change with long-term increased drought severity? *Plant, Cell & Environment*, 33(5):863–875, 2010b. ISSN

1365-3040. https://doi.org/10.1111/j.1365-3040.2009.02112.x. URL https://onlinelibrary.wiley.com/doi/abs/10.1111/j.1365-3040.2009.02112.x.

Jean-Marc Limousin, Amélie Roussel, Jesús Rodríguez-Calcerrada, José M. Torres-Ruiz, Myriam Moreno, Laura Garcia de Jalon, Jean-Marc Ourcival, Guillaume Simioni, Hervé Cochard, and Nicolas Martin-StPaul. Drought acclimation of Quercus ilex leaves improves tolerance to moderate drought but not resistance to severe water stress. *Plant, Cell & Environment*, 45(7):1967–1984, 2022. ISSN 1365-3040. https://doi.org/10.1111/pce.14326. URL https://onlinelibrary.wiley.com/doi/abs/10.1111/pce.14326. _eprint: https://onlinelibrary.wiley.com/doi/pdf/10.1111/pce.14326.

Hongyan Liu, Chongyang Xu, Craig D. Allen, Henrik Hartmann, Xiaohua Wei, Dan Yakir, Xiuchen Wu, and Pengtao Yu. Nature-based framework for sustainable afforestation in global drylands under changing climate. *Global Change Biology*, 28(7):2202–2220, 2022. https://doi.org/10.1111/gcb.16059. URL https://doi.org/10.1111/gcb.16059. Hongyan Liu and Chongyang Xu are joint first authors.

Isabelle Maréchaux, Damien Bonal, Megan K. Bartlett, Benoît Burban, Sabrina Coste, Elodie A. Courtois, Maguy Dulormne, and et al. Dry-season decline in tree sapflux is correlated with leaf turgor loss point in a tropical rainforest. *Functional Ecology*, 32(10):2285–2297, 2018. https://doi.org/10.1111/1365-2435.13188. URL https://doi.org/10.1111/1365-2435.13188.

Jalal Matar, Maria J Sanjuan-Ferrer, Marc Rodriguez-Cassola, Susan Steele-Dunne, and Francesco De Zan. A Concept for an Interferometric SAR Mission with Sub-daily Revisit. In *15th European Conference on Synthetic Aperture Radar, EUSAR 2024*, pages 18–22. IEEE, 2024.

K.C. Mcdonald, M.C. Dobson, and F.T. Ulaby. Using Mimics To Model L-band Multiangle and Multitemporal Backscatter From A Walnut Orchard. *IEEE Transactions on Geoscience and Remote Sensing*, 28(4):477–491, July 1990. ISSN 1558-0644. https://doi.org/10.1109/TGRS.1990.572925.

Nate G. McDowell, Gerard Sapes, Alexandria Pivovaroff, Henry D. Adams, Craig D. Allen, William R. L. Anderegg, Matthias Arend, David D. Breshears, Tim Brodribb, Brendan Choat, Hervé Cochard, Miquel De Cáceres, Martin G. De Kauwe, Charlotte Grossiord, William M. Hammond, Henrik Hartmann, Günter Hoch, Ansgar Kahmen, Tamir Klein, D. Scott Mackay, Marylou Mantova, Jordi Martínez-Vilalta, Belinda E. Medlyn, Maurizio Mencuccini, Andrea Nardini, Rafael S. Oliveira, Anna Sala, David T. Tissue, José M. Torres-Ruiz, Amy M. Trowbridge, Anna T. Trugman, Erin Wiley, and Chonggang Xu. Mechanisms of woody-plant mortality under rising drought, CO2 and vapour pressure deficit. *Nature Reviews Earth & Environment*, 3(5):294–308, May 2022. ISSN 2662-138X. https://doi.org/10.1038/s43017-022-00272-1. URL https://doi.org/10.1038/s43017-022-00272-1.

Laurent Misson, David Degueldre, Christian Collin, Raquel Rodriguez, Alain Rocheteau, Jean-Marc Ourcival, and Serge Rambal. Phenological responses to extreme droughts in a Mediterranean forest. *Global Change Biology*, 17(2):1036–1048, 2011. ISSN 1365-2486. https://doi.org/10.1111/j.1365-2486.2010.02348.x. URL https://onlinelibrary.wiley.com/doi/abs/10.1111/j.1365-2486.2010.02348.x. _eprint: https://onlinelibrary.wiley.com/doi/pdf/10.1111/j.1365-2486.2010.02348.x.

Mostafa Momen, Jeffrey D. Wood, Kimberly A. Novick, Robert Pangle, William T. Pockman, Nate G. McDowell, and Alexandra G. Konings. Interacting Effects of Leaf Water Potential and Biomass on Vegetation Optical Depth. *Journal of Geophysical Research: Biogeosciences*, 122(11):3031–3046, 2017. ISSN 2169-8961. https://doi.org/10.1002/2017JG004145. URL https://onlinelibrary.wiley.com/doi/abs/10.1002/2017JG004145. _eprint: https://onlinelibrary.wiley.com/doi/pdf/10.1002/2017JG004145.

Albert R. Monteith and Lars M. H. Ulander. A Tower-Based Radar Study of Temporal Coherence of a Boreal Forest at P-, L-, and C-Bands and Linear Cross Polarization. *IEEE Transactions on Geoscience and Remote Sensing*, 60:1–15, 2022. ISSN 1558-0644. https://doi.org/10.1109/TGRS.2021.3074098.

N. Ouaadi, L. Villard, J. Ezzahar, P.L. Frison, S. Khabba, M. Kasbani, P. Fanise, A. Chakir, V. Le Dantec, S. Er-Raki, and L. Jarlan. Diurnal cycles of c-band temporal coherence and backscattering coefficient over a wheat field in a semi-arid area. In *2021 IEEE International Geoscience and Remote Sensing Symposium IGARSS*, pages 3817–3820, 2021. https://doi.org/10.1109/IGARSS47720.2021.9553586.

Aaron C. Paget, David G. Long, and Nathan M. Madsen. RapidScat Diurnal Cycles Over Land. *IEEE Transactions on Geoscience and Remote Sensing*, 54(6):3336–3344, June 2016. ISSN 1558-0644. https://doi.org/10.1109/TGRS.2016.2515022.

Gilberto Pastorello, Carlo Trotta, Eleonora Canfora, Housen Chu, Danielle Christianson, You-Wei Cheah, Cristina Poindexter, Jiquan Chen, Abdelrahman Elbashandy, Marty Humphrey, Peter Isaac, Diego Polidori, Alessio Ribeca, Catharine van Ingen, Leiming Zhang, Brian Amiro, Christof Ammann, M. Altaf Arain, Jonas Ardö, Timothy Arkebauer, Stefan K. Arndt, Nicola Arriga, Marc Aubinet, Mika Aurela, Dennis Baldocchi, Alan Barr, Eric Beamesderfer, Luca Belelli Marchesini, Onil Bergeron, Jason Beringer, Christian Bernhofer, Daniel Berveiller, Dave Billesbach, Thomas Andrew Black, Peter D. Blanken, Gil Bohrer, Julia Boike, Paul V. Bolstad, Damien Bonal, Jean-Marc Bonnefond, David R. Bowling, Rosvel Bracho, Jason Brodeur, Christian Brümmer, Nina Buchmann, Benoit Burban, Sean P. Burns, Pauline Buysse, Peter Cale, Mauro Cavagna, Pierre Cellier, Shiping Chen, Isaac Chini, Torben R. Christensen, James Cleverly, Alessio Collalti, Claudia Consalvo, Bruce D. Cook, David Cook, Carole Coursolle, Edoardo Cremonese, Peter S. Curtis, Ettore D'Andrea, Humberto da Rocha, Xiaoqin Dai, Kenneth J. Davis, Bruno De Cinti, Agnes de Grandcourt, Anne De Ligne, Raimundo C. De Oliveira, Nicolas Delpierre, Ankur R. Desai, Carlos Marcelo Di Bella, Paul di Tommasi, Han Dolman, Francisco Domingo, Gang Dong, Sabina Dore, Pierpaolo Duce, Eric Dufrêne, Allison Dunn, Jiří Dušek, Derek Eamus, Uwe Eichelmann, Hatim Abdalla M. ElKhidir, Werner Eugster, Cacilia M. Ewenz, Brent Ewers, Daniela Famulari, Silvano Fares, Iris Feigenwinter, Andrew Feitz, Rasmus Fensholt, Gianluca Filippa, Marc Fischer, John Frank, Marta Galvagno, Mana Gharun, Damiano Gianelle, Bert Gielen, Beniamino Gioli, Anatoly Gitelson, Ignacio Goded, Mathias Goeckede, Allen H. Goldstein, Christopher M. Gough, Michael L. Goulden, Alexander Graf, Anne Griebel, Carsten Gruening, Thomas Grünwald, Albin Hammerle, Shijie Han, Xingguo Han, Birger Ulf Hansen, Chad Hanson, Juha Hatakka, Yongtao He, Markus Hehn, Bernard Heinesch, Nina Hinko-Najera, Lukas Hörtnagl, Lindsay Hutley, Andreas Ibrom, Hiroki Ikawa, Marcin Jackowicz-Korczynski, Dalibor Janouš, Wilma Jans, Rachhpal Jassal, Shicheng Jiang, Tomomichi Kato, Myroslava Khomik, Janina Klatt, Alexander Knohl, Sara Knox, Hideki Kobayashi, Georgia Koerber, Olaf Kolle, Yoshiko Kosugi, Ayumi Kotani, Andrew Kowalski, Bart Kruijt, Julia Kurbatova, Werner L. Kutsch, Hyojung Kwon, Samuli Launiainen, Tuomas Laurila, Bev Law, Ray Leuning, Yingnian Li, Michael Liddell, Jean-Marc Limousin, Marryanna Lion, Adam J. Liska, Annalea Lohila, Ana López-Ballesteros, Efrén López-Blanco, Benjamin Loubet, Denis Loustau, Antje Lucas-Moffat, Johannes Lüers, Siyan Ma, Craig Macfarlane, Vincenzo Magliulo, Regine Maier, Ivan Mammarella, Giovanni Manca, Barbara Marcolla, Hank A. Margolis, Serena Marras, William Massman, Mikhail Mastepanov, Roser Matamala, Jaclyn Hatala Matthes, Francesco Mazzenga, Harry McCaughey, Ian McHugh, Andrew M. S. McMillan, Lutz Merbold, Wayne Meyer, Tilden Meyers, Scott D. Miller, Stefano Minerbi, Uta Moderow, Russell K. Monson, Leonardo Montagnani, Caitlin E. Moore, Eddy Moors, Virginie Moreaux, Christine Moureaux, J. William Munger, Taro Nakai, Johan Neirynck, Zoran Nesic, Giacomo Nicolini, Asko Noormets, Matthew Northwood, Marcelo Nosetto, Yann Nouvellon, Kimberly Novick, Walter Oechel, Jørgen Eivind Olesen, Jean-Marc Ourcival, Shirley A. Papuga, Frans-Jan Parmentier, Eugenie Paul-Limoges, Marian Pavelka, Matthias Peichl, Elise Pendall, Richard P. Phillips, Kim Pilegaard, Norbert Pirk, Gabriela Posse, Thomas Powell, Heiko Prasse, Suzanne M. Prober, Serge Rambal, Üllar Rannik, Naama Raz-Yaseef, David Reed, Victor Resco de Dios, Natalia Restrepo-Coupe, Borja R. Reverter, Marilyn Roland, Simone Sabbatini, Torsten Sachs, Scott R. Saleska, Enrique P. Sánchez-Cañete, Zulia M. Sanchez-Mejia, Hans Peter Schmid, Marius Schmidt, Karl Schneider, Frederik Schrader, Ivan Schroder, Russell L. Scott, Pavel Sedlák, Penélope Serrano-Ortíz, Changliang Shao, Peili Shi, Ivan Shironya, Lukas Siebicke, Ladislav Šigut, Richard Silberstein, Costantino Sirca, Donatella Spano, Rainer Steinbrecher, Robert M. Stevens, Cove Sturtevant, Andy Suyker, Torbern Tagesson, Satoru Takanashi, Yanhong Tang, Nigel Tapper, Jonathan Thom, Frank Tiedemann, Michele

Tomassucci, Juha-Pekka Tuovinen, Shawn Urbanski, Riccardo Valentini, Michiel van der Molen, Eva van Gorsel, Ko van Huissteden, Andrej Varlagin, Joseph Verfaillie, Timo Vesala, Caroline Vincke, Domenico Vitale, Natalia Vygodskaya, Jeffrey P. Walker, Elizabeth Walter-Shea, Huimin Wang, Robin Weber, Sebastian Westermann, Christian Wille, Steven Wofsy, Georg Wohlfahrt, Sebastian Wolf, William Woodgate, Yuelin Li, Roberto Zampedri, Junhui Zhang, Guoyi Zhou, Donatella Zona, Deb Agarwal, Sebastien Biraud, Margaret Torn, and Dario Papale. The FLUXNET2015 dataset and the ONEFlux processing pipeline for eddy covariance data. *Scientific Data*, 7 (1):225, July 2020. ISSN 2052-4463. https://doi.org/10.1038/s41597-020-0534-3. URL https://doi.org/10.1038/s41597-020-0534-3.

José Javier Peguero-Pina, Alberto Vilagrosa, David Alonso-Forn, Juan Pedro Ferrio, Domingo Sancho-Knapik, and Eustaquio Gil-Pelegrín. Living in drylands: Functional adaptations of trees and shrubs to cope with high temperatures and water scarcity. *Forests*, 11(10):1028, 2020. https://doi.org/10.3390/f11101028. URL https://doi.org/10.3390/f11101028. Special Issue: Mechanisms of Adaptation of Trees and Shrubs to Dry and Hot Environments.

Drew M. P. Peltier and Kiona Ogle. Still recovering or just remembering? To understand drought legacies, modelling choices matter. *Journal of Ecology*, 111(6):1170–1173, June 2023. ISSN 0022-0477, 1365-2745. https://doi.org/10.1111/1365-2745.14116. URL https://besjournals.onlinelibrary.wiley.com/doi/10.1111/1365-2745.14116.

Rafael Poyatos, Víctor Granda, Roberto Molowny-Horas, Maurizio Mencuccini, Kathy Steppe, and Jordi Martínez-Vilalta. SAPFLUXNET: towards a global database of sap flow measurements. *Tree Physiology*, 36(12):1449–1455, December 2016. ISSN 0829-318X. https://doi.org/10.1093/treephys/tpw110. URL https://doi.org/10.1093/treephys/tpw110.

Rafael Poyatos, Víctor Granda, Víctor Flo, Roberto Molowny-Horas, Kathy Steppe, Maurizio Mencuccini, and Jordi Martínez-Vilalta. Sapfluxnet: A global database of sap flow measurements, March 2019. URL https://doi.org/10.5281/zenodo.2530798.

Rafael Poyatos, Víctor Granda, Víctor Flo, Mark A. Adams, Balázs Adorján, David Aguadé, Marcos P. M. Aidar, Scott Allen, M. Susana Alvarado-Barrientos, Kristina J. Anderson-Teixeira, Luiza Maria Aparecido, M. Altaf Arain, Ismael Aranda, Heidi Asbjornsen, Robert Baxter, Eric Beamesderfer, Z. Carter Berry, Daniel Berveiller, Bethany Blakely, Johnny Boggs, Gil Bohrer, Paul V. Bolstad, Damien Bonal, Rosvel Bracho, Patricia Brito, Jason Brodeur, Fernando Casanoves, Jérôme Chave, Hui Chen, Cesar Cisneros, Kenneth Clark, Edoardo Cremonese, Hongzhong Dang, Jorge S. David, Teresa S. David, Nicolas Delpierre, Ankur R. Desai, Frederic C. Do, Michal Dohnal, Jean-Christophe Domec, Sebinasi Dzikiti, Colin Edgar, Rebekka Eichstaedt, Tarek S. El-Madany, Jan Elbers, Cleiton B. Eller, Eugénie S. Euskirchen, Brent Ewers, Patrick Fonti, Alicia Forner, David I. Forrester, Helber C. Freitas, Marta Galvagno, Omar Garcia-Tejera, Chandra Prasad Ghimire, Teresa E. Gimeno, John Grace, André Granier, Anne Griebel, Yan Guangyu, Mark B. Gush, Paul J. Hanson, Niles J. Hasselquist, Ingo Heinrich, Virginia Hernandez-Santana, Valentine Herrmann, Teemu Hölttä, Friso Holwerda, James Irvine, Supat Isarangkool Na Ayutthaya, Paul G. Jarvis, Hubert Jochheim, Carlos A. Joly, Julia Kaplick, Hyun Seok Kim, Leif Klemedtsson, Heather Kropp, Fredrik Lagergren, Patrick Lane, Petra Lang, Andrei Lapenas, Víctor Lechuga, Minsu Lee, Christoph Leuschner, Jean-Marc Limousin, Juan Carlos Linares, Maj-Lena Linderson, Anders Lindroth, Pilar Llorens, Álvaro López-Bernal, Michael M. Loranty, Dietmar Lüttschwager, Cate Macinnis-Ng, Isabelle Maréchaux, Timothy A. Martin, Ashley Matheny, Nate McDowell, Sean McMahon, Patrick Meir, Ilona Mészáros, Mirco Migliavacca, Patrick Mitchell, Meelis Mölder, Leonardo Montagnani, Georgianne W. Moore, Ryogo Nakada, Furong Niu, Rachael H. Nolan, Richard Norby, Kimberly Novick, Walter Oberhuber, Nikolaus Obojes, A. Christopher Oishi, Rafael S. Oliveira, Ram Oren, Jean-Marc Ourcival, Teemu Paljakka, Oscar Perez-Priego, Pablo L. Peri, Richard L. Peters, Sebastian Pfautsch, William T. Pockman, Yakir Preisler, Katherine Rascher, George Robinson, Humberto Rocha, Alain Rocheteau, Alexander Röll, Bruno H. P. Rosado, Lucy Rowland, Alexey V. Rubtsov, Santiago Sabaté, Yann Salmon, Roberto L. Salomón, Elisenda Sánchez-Costa, Karina V. R. Schäfer, Bernhard Schuldt, Alexandr Shashkin, Clément Stahl, Marko Stojanović, Juan Carlos Suárez, Ge Sun, Justyna Szatniewska, Fyodor Tatarinov, Miroslav Tesař, Frank M. Thomas, Pantana Tor-ngern, Josef Urban, Fernando Valladares, Christiaan van der

Tol, Ilja van Meerveld, Andrej Varlagin, Holm Voigt, Jeffrey Warren, Christiane Werner, Willy Werner, Gerhard Wieser, Lisa Wingate, Stan Wullschleger, Koong Yi, Roman Zweifel, Kathy Steppe, Maurizio Mencuccini, and Jordi Martínez-Vilalta. Global transpiration data from sap flow measurements: the SAPFLUXNET database. *Earth System Science Data*, 13(6):2607–2649, June 2021. ISSN 1866-3508. https://doi.org/10.5194/essd-13-2607-2021. URL https://essd.copernicus.org/articles/13/2607/2021/. Publisher: Copernicus GmbH.

Yakir Preisler, Fedor Tatarinov, José M. Grünzweig, and Dan Yakir. Seeking the "point of no return" in the sequence of events leading to mortality of mature trees. *Plant, Cell & Environment*, 44(5):1315–1328, 2021. ISSN 1365-3040. https://doi.org/10.1111/pce.13942. URL https://onlinelibrary.wiley.com/doi/abs/10.1111/pce.13942. _eprint: https://onlinelibrary.wiley.com/doi/pdf/10.1111/pce.13942.

Catherine Prigent, Carlos Jimenez, Lan Anh Dinh, Frédéric Frappart, Pierre Gentine, Jean-Pierre Wigneron, and Joseph Munchak. Diurnal and Seasonal Variations of Passive and Active Microwave Satellite Observations Over Tropical Forests. *Journal of Geophysical Research: Biogeosciences*, 127(2):e2021JG006677, 2022. ISSN 2169-8961. https://doi.org/10.1029/2021JG006677. URL https://onlinelibrary.wiley.com/doi/abs/10.1029/2021JG006677.

Heidi J. Renninger, Leah F. Stewart, and Randall J. Rousseau. Water use, efficiency, and stomatal sensitivity in eastern cottonwood and hybrid poplar varietals on contrasting sites in the southeastern united states. *Frontiers in Forests and Global Change*, Volume 4 - 2021, 2021. ISSN 2624-893X. https://doi.org/10.3389/ffgc.2021.704799. URL https://www.frontiersin.org/journals/forests-and-global-change/articles/10.3389/ffgc.2021.704799.

ICOS RI. Ecosystem final quality (L2) product in ETC-Archive format - release 2022-1. June 2022. https://doi.org/10.18160/PAD9-HQHU. URL https://meta.icos-cp.eu/collections/-ZrCo_Cousoqvxnlvz83l0K4.

L. Rowland, A. C. L. da Costa, D. R. Galbraith, R. S. Oliveira, O. J. Binks, A. a. R. Oliveira, A. M. Pullen, C. E. Doughty, D. B. Metcalfe, S. S. Vasconcelos, L. V. Ferreira, Y. Malhi, J. Grace, M. Mencuccini, and P. Meir. Death from drought in tropical forests is triggered by hydraulics not carbon starvation. *Nature*, 528(7580):119–122, December 2015. ISSN 1476-4687. https://doi.org/10.1038/nature15539. URL https://www.nature.com/articles/nature15539. Publisher: Nature Publishing Group.

Nadine K. Ruehr, Andreas Gast, Christina Weber, Bärbel Daub, and Almut Arneth. Water availability as dominant control of heat stress responses in two contrasting tree species. *Tree Physiology*, 36(2):164–178, 2015. ISSN 0829-318X. https://doi.org/10.1093/treephys/tpv102. URL https://doi.org/10.1093/treephys/tpv102.

Nadine K. Ruehr, Rüdiger Grote, Stefan Mayr, and Almut Arneth. Beyond the extreme: Recovery of carbon and water relations in woody plants following heat and drought stress. *Tree Physiology*, 39(8):1285–1299, 2019. ISSN 1758-4469. https://doi.org/10.1093/treephys/tpz032. URL https://doi.org/10.1093/treephys/tpz032.

Julien Ruffault, Jean-Marc Limousin, François Pimont, Jean-Luc Dupuy, Miquel De Càceres, Hervé Cochard, Florent Mouillot, Chris J. Blackman, José M. Torres-Ruiz, Russell A. Parsons, Myriam Moreno, Sylvain Delzon, Steven Jansen, Albert Olioso, Brendan Choat, and Nicolas Martin-StPaul. Plant hydraulic modelling of leaf and canopy fuel moisture content reveals increasing vulnerability of a Mediterranean forest to wildfires under extreme drought. *New Phytologist*, 237(4):1256–1269, 2023. ISSN 1469-8137. https://doi.org/10.1111/nph.18614. URL https://onlinelibrary.wiley.com/doi/abs/10.1111/nph.18614. _eprint: https://nph.onlinelibrary.wiley.com/doi/pdf/10.1111/nph.18614.

S.S. Saatchi and M. Moghaddam. Estimation of crown and stem water content and biomass of boreal forest using polarimetric sar imagery. *IEEE Transactions on Geoscience and Remote Sensing*, 38(2):697–709, 2000. https://doi.org/10.1109/36.841999.

Marc Schneebeli, Sebastian Wolf, Norbert Kunert, Werner Eugster, and Christian Mätzler. Relating the X-band opacity of a tropical tree canopy to sapflow, rain interception and dew formation. *Remote Sensing of Environment*, 115(8):2116–2125, August 2011. ISSN 0034-4257. https://doi.org/10.1016/j.rse.2011.04.016. URL https://www.sciencedirect.com/science/article/pii/S0034425711001441.

Stanislaus J. Schymanski, Dani Or, and Maciej Zwieniecki. Stomatal control and leaf thermal and hydraulic capacitances under rapid environmental fluctuations. *PLOS ONE*, 8(1):e54231, 2013. https://doi.org/10.1371/journal.pone.0054231. URL https://doi.org/10.1371/journal.pone.0054231.

Rupert Seidl, Dominik Thom, Markus Kautz, Dario Martin-Benito, Mikko Peltoniemi, Giorgio Vacchiano, Jan Wild, Davide Ascoli, Michal Petr, Juha Honkaniemi, Manfred J. Lexer, Volodymyr Trotsiuk, Paola Mairota, Miroslav Svoboda, Marek Fabrika, Thomas A. Nagel, and Christopher P.O. Reyer. Forest disturbances under climate change. *Nature Climate Change*, 7(6):395–402, June 2017. ISSN 17586798. https://doi.org/10.1038/NCLIMATE3303.

Mahmoud F. Seleiman, Nasser Al-Suhaibani, Nawab Ali, Mohammad Akmal, Majed Alotaibi, Yahya Refay, Turgay Dindaroglu, Hafiz Haleem Abdul-Wajid, and Martin Leonardo Battaglia. Drought stress impacts on plants and different approaches to alleviate its adverse effects. *Plants*, 10(2):259, 2021. https://doi.org/10.3390/plants10020259. URL https://doi.org/10.3390/plants10020259. Special Issue: Water Stress and Desiccation Tolerance in Plants.

Gustavo C. Spanner, Bruno O. Gimenez, Cynthia L. Wright, Valdiek Silva Menezes, Brent D. Newman, Adam D. Collins, Kolby J. Jardine, Robinson I. Negrón-Juárez, Adriano José Nogueira Lima, Jardel Ramos Rodrigues, Jeffrey Q. Chambers, Niro Higuchi, and Jeffrey M. Warren. Dry season transpiration and soil water dynamics in the central amazon. *Frontiers in Plant Science*, 13:825097, 2022. ISSN 1664-462X. https://doi.org/10.3389/fpls.2022.825097. URL https://www.frontiersin.org/journals/plant-science/articles/10.3389/fpls.2022.825097.

John S. Sperry and David M. Love. What plant hydraulics can tell us about responses to climate-change droughts. *New Phytologist*, 207(1): 14–27, 2015. https://doi.org/10.1111/nph.13354. URL https://doi.org/10.1111/nph.13354.

S. C. Steele-Dunne, J. Friesen, and N. van de Giesen. Using Diurnal Variation in Backscatter to Detect Vegetation Water Stress. *IEEE Transactions on Geoscience and Remote Sensing*, 50(7):2618–2629, July 2012. ISSN 1558-0644. https://doi.org/10.1109/TGRS.2012.2194156.

Susan Steele-Dunne, Ana Basto, Francesco de Zan, Wouter Dorigo, Stef Lhermitte, Christian Massari, Jalal Matar, David Milodowski, Diego Miralle, Albert Monteith, Marc Rodriguez Cassola, Christopher Taylor, Stefano Tebaldin, and Lars Ulander. SLAINTE: A SAR mission concept for sub-daily microwave remote sensing of vegetation. In *EUSAR 2024; 15th European Conference on Synthetic Aperture Radar*, pages 870–872, April 2024. URL https://ieeexplore.ieee.org/document/10659518?arnumber=10659518.

Juan Carlos Suárez, Fernando Casanoves, Marie Ange Ngo Bieng, Luz Marina Melgarejo, Julio A. Di Rienzo, and Cristina Armas. Prediction model for sap flow in cacao trees under different radiation intensities in the western colombian amazon. *Scientific Reports*, 11(1):10512, 2021. ISSN 2045-2322. https://doi.org/10.1038/s41598-021-89876-z. URL https://doi.org/10.1038/s41598-021-89876-z.

Nadezhda M. Tchebakova, Viacheslav I. Zyryanov, Olga A. Zyryanova, Elena I. Parfenova, Takuya Kajimoto, and Yojiro Matsuura. A Comparative Study of Climatology, Energy and Mass Exchange in Two Forests on Contrasting Habitats in Central Siberia: Permafrost Larix gmelinii vs. Permafrost-Free Pinus sylvestris. *Forests*, 14(2):346, February 2023. ISSN 1999-4907. https://doi.org/10.3390/f14020346. URL https://www.mdpi.com/1999-4907/14/2/346. Number: 2 Publisher: Multidisciplinary Digital Publishing Institute.

José M. Torres-Ruiz, Hervé Cochard, Sylvain Delzon, Thomas Boivin, Regis Burlett, Maxime Cailleret, Déborah Corso, Chloé E. L. Delmas, Miquel De Caceres, Antonio Diaz-Espejo, Pilar Fernández-Conradi, Joannes Guillemot, Laurent J. Lamarque, Jean-Marc Limousin, Marylou Mantova, Maurizio Mencuccini, Xavier Morin, François Pimont, Victor Resco De Dios, Julien Ruffault, Santiago Trueba, and Nicolas K. Martin-StPaul. Plant hydraulics at the heart of plant, crops and ecosystem functions in the face of climate change. 241(3): 984–999. ISSN 1469-8137. https://doi.org/10.1111/nph.19463. URL https://onlinelibrary.wiley.com/doi/abs/10.1111/nph.19463. _eprint: https://nph.onlinelibrary.wiley.com/doi/pdf/10.1111/nph.19463.

Melvin T. Tyree and Frank W. Ewers. The hydraulic architecture of trees and other woody plants. *New Phytologist*, 119(3):345–360, 1991. ISSN 1469-8137. https://doi.org/10.1111/j.1469-8137.1991.tb00035.x. URL https://onlinelibrary.wiley.com/doi/abs/10.1111/j.1469-8137.1991.tb00035.x. _eprint: https://nph.onlinelibrary.wiley.com/doi/pdf/10.1111/j.1469-8137.1991.tb00035.x.

Lars M. H. Ulander and Albert R. Monteith. BorealScat Final Report (Contract Change Notice 1). ESA, 2022.

Lars M. H. Ulander, Albert R. Monteith, and Martin Rönnfalk. BorealScat Final Report. ESA, 2019. https://doi.org/https://doi.org/10.57780/esa-e071d3d.

Josef Urban, Miles Ingwers, Mary Anne McGuire, and Robert O. Teskey. Stomatal conductance increases with rising temperature. *Plant Signaling & Behavior*, 12(8):e1356534, 2017. https://doi.org/10.1080/15592324.2017.1356534. URL https://doi.org/10.1080/15592324.2017.1356534. PMID: 28786730.

Josef Urban, Alexey V. Rubtsov, Anastasiya V. Urban, Alexander V. Shashkin, and Vera E. Benkova. Canopy transpiration of a *Larix sibirica* and *Pinus sylvestris* forest in Central Siberia. *Agricultural and Forest Meteorology*, 271:64–72, June 2019. ISSN 0168-1923. https://doi.org/10.1016/j.agrformet.2019.02.038. URL https://www.sciencedirect.com/science/article/pii/S0168192319300930.

P. C. Vermunt, S. C. Steele-Dunne, S. Khabbazan, J. Judge, and N. C. van de Giesen. Extrapolating continuous vegetation water content to understand sub-daily backscatter variations. *Hydrology and Earth System Sciences*, 26(5):1223–1241, 2022. https://doi.org/10.5194/hess-26-1223-2022. URL https://hess.copernicus.org/articles/26/1223/2022/.

Paul C. Vermunt, Saeed Khabbazan, Susan C. Steele-Dunne, Jasmeet Judge, Alejandro Monsivais-Huertero, Leila Guerriero, and Pang-Wei Liu. Response of subdaily l-band backscatter to internal and surface canopy water dynamics. *IEEE Transactions on Geoscience and Remote Sensing*, 59(9):7322–7337, 2021. https://doi.org/10.1109/TGRS.2020.3035881.

Sergio M. Vicente-Serrano, Diego G. Miralles, Nate McDowell, Tim Brodribb, Fernando Domínguez-Castro, Ruby Leung, and Akash Koppa. The uncertain role of rising atmospheric CO2 on global plant transpiration. *Earth-Science Reviews*, 230:104055, July 2022a. ISSN 0012-8252. https://doi.org/10.1016/j.earscirev.2022.104055. URL https://www.sciencedirect.com/science/article/pii/S0012825222001398.

Sergio M. Vicente-Serrano, Dhais Peña-Angulo, Santiago Beguería, Fernando Domínguez-Castro, Miquel Tomás-Burguera, Iván Noguera, Luis Gimeno-Sotelo, and Ahmed El Kenawy. Global drought trends and future projections. *Philosophical Transactions of the Royal Society A: Mathematical, Physical and Engineering Sciences*, 380(2238):20210285, October 2022b. https://doi.org/10.1098/rsta.2021.0285. URL https://royalsocietypublishing.org/doi/full/10.1098/rsta.2021.0285.

Liuliu Wan, Quan Zhang, Lei Cheng, Yujie Liu, Shujing Qin, Jijun Xu, and Yongqiang Wang. What determines the time lags of sap flux with solar radiation and vapor pressure deficit? *Agricultural and Forest Meteorology*, 333:109414, April 2023. ISSN 0168-1923. https://doi.org/10.1016/j.agrformet.2023.109414. URL https://www.sciencedirect.com/science/article/pii/S0168192323001065.

William D. Wheeler, Brent Black, and Bruce Bugbee. Assessing water stress in a high-density apple orchard using trunk circumference variation, sap flow index and stem water potential. *Frontiers in Plant Science*, 14:1214429, 2023. https://doi.org/10.3389/fpls.2023.1214429. URL https://doi.org/10.3389/fpls.2023.1214429.

Shiqin Xu, Tim R. McVicar, Lingcheng Li, Zhongbo Yu, Peng Jiang, Yuliang Zhang, Zhaoxin Ban, Wanqiu Xing, Ningpeng Dong, Hua Zhang, and Mingjun Zhang. Globally assessing the hysteresis between sub-diurnal actual evaporation and vapor pressure deficit at the ecosystem scale: Patterns and mechanisms. *Agricultural and Forest Meteorology*, 323:109085, August 2022. ISSN 0168-1923. https://doi.org/10.1016/j.agrformet.2022.109085. URL https://www.sciencedirect.com/science/article/pii/S0168192322002738.

Han Zheng, Qiufeng Wang, Xianjin Zhu, Yingnian Li, and Guirui Yu. Hysteresis Responses of Evapotranspiration to Meteorological Factors at a Diel Timescale: Patterns and Causes. *PLOS ONE*, 9(6):e98857, June 2014. ISSN 1932-6203.

https://doi.org/10.1371/journal.pone.0098857. URL https://journals.plos.org/plosone/article?id=10.1371/journal.pone.0098857. Publisher: Public Library of Science.

Ruxandra-Maria Zotta, Leander Moesinger, Robin van der Schalie, Mariette Vreugdenhil, Wolfgang Preimesberger, Thomas Frederikse, Richard de Jeu, and Wouter Dorigo. VODCA v2: multi-sensor, multi-frequency vegetation optical depth data for long-term canopy dynamics and biomass monitoring. *Earth System Science Data*, 16(10):4573–4617, October 2024. ISSN 1866-3508. https://doi.org/10.5194/essd-16-4573-2024. URL https://essd.copernicus.org/articles/16/4573/2024/. Publisher: Copernicus GmbH.

G. Zuecco, D. Penna, M. Borga, and H. J. van Meerveld. A versatile index to characterize hysteresis between hydrological variables at the runoff event timescale. *Hydrological Processes*, 30(9):1449–1466, 2016. ISSN 1099-1085. https://doi.org/10.1002/hyp.10681. URL https://onlinelibrary.wiley.com/doi/abs/10.1002/hyp.10681. _eprint: https://onlinelibrary.wiley.com/doi/pdf/10.1002/hyp.10681.